Article

Mechanism of Photoinduced Metal-Free Atom Transfer Radical Polymerization: Experimental and Computational Studies

Xiangcheng Pan, Cheng Fang, Marco Fantin, Nikhil Malhotra , Woong Young So, Linda A. Peteanu, Abdirisak A. Isse, Armando Gennaro, Peng Liu, and Krzysztof Matyjaszewski

J. Am. Chem. Soc., **Just Accepted Manuscript** • DOI: 10.1021/jacs.5b13455 • Publication Date (Web): 28 Jan 2016

Mechanism of Photoinduced Metal-Free Atom Transfer Radical Polymerization: Experimental and Computational Studies

Xiangcheng Pan[1], Cheng Fang[2], Marco Fantin[1,3], Nikhil Malhotra[1], Woong Young So[1], Linda A. Peteanu[1], Abdirisak A. Isse[3], Armando Gennaro[3,*], Peng Liu[2,*], and Krzysztof Matyjaszewski[1,*]

[1]Department of Chemistry, Carnegie Mellon University, Pittsburgh, Pennsylvania, 15213, United States

[2]Department of Chemistry, University of Pittsburgh, Pittsburgh, Pennsylvania, 15260, United States

[3]Department of Chemical Sciences, University of Padova, via Marzolo 1, 35131 Padova, Italy

ABSTRACT: Photoinduced metal-free atom transfer radical polymerization (ATRP) of methyl methacrylate was investigated using several phenothiazine derivatives and other related compounds as photoredox catalysts. The experiments show that all selected catalysts can be involved in the activation step, but not all of them participated efficiently in the deactivation step. The redox properties and the stability of radical cations derived from the catalysts were evaluated by cyclic voltammetry. Laser flash photolysis (LFP) was used to determine the lifetime and activity of photoexcited catalysts. Kinetic analysis of the activation reaction according to dissociative electron transfer (DET) theory suggests that the activation occurs only with an excited state of catalyst. Density functional theory (DFT) calculations revealed the structures and stabilities of the radical cation intermediates as well as the reaction energy profiles of deactivation pathways with different photoredox catalysts. Both experiments and calculations suggest that the activation process undergoes a DET mechanism while an associative electron transfer involving a termolecular encounter (the exact reverse of DET pathway) is favored in the deactivation process. This detailed study provides a deeper understanding of the chemical processes of metal-free ATRP that can aid the design of better catalytic systems. Additionally, this work elucidates several important common pathways involved in synthetically useful organic reactions catalyzed by photoredox catalysts.

INTRODUCTION

Reversible deactivation radical polymerization (RDRP) procedures, also termed controlled or living radical polymerization, (CRP or LRP), provide well-defined polymers with complex architectures.[1] RDRP methods include nitroxide-mediated polymerization (NMP),[2] atom transfer radical polymerization (ATRP),[3] and reversible addition−fragmentation chain-transfer (RAFT) polymerization.[4] ATRP is the most extensively used and widely investigated method due to the commercial availability of various initiators and catalysts.

Control over the polymer structure and suppression of radical termination in an ATRP are due to a concurrent growth of all chains and fast activation/deactivation equilibrium in which a transition metal complex (usually $[Cu^{I}L]^{+}$, L = ligand) activates reversibly an alkyl halide (P_n-X, X = Br or Cl), providing an alkyl radical and the metal complex in a higher oxidation state $[X–Cu^{II}L]^{+}$ (Scheme 1a).[5] The alkyl radical could add up to a few monomer units before it abstracts the halogen back from a deactivator $[X–Cu^{II}L]^{+}$ to reform the dormant alkyl halide and the activator $[Cu^{I}L]^{+}$. Originally, ATRP required relatively large concentrations (1,000 to 10,000 ppm) of Cu-based catalysts to compensate for radical termination reactions and due to relatively low activities of the catalyst complexes. Significant progress has been recently achieved allowing use of low ppm levels of Cu catalysts in ATRP (Scheme 1b).[6] These systems employ reducing agents for activators regenerated by electron transfer (ARGET) ATRP,[7] conventional radical initiators as in initiators for continuous activator regeneration (ICAR) ATRP,[8] or zerovalent metals as supplemental activators and reducing agents (SARA) ATRP,[9] also termed SET-LRP.[10] Additionally, nonchemical methods such as electrochemically mediated ATRP (*e*ATRP)[11] and photochemically mediated ATRP (photoATRP)[12] were developed to regulate the polymerization by controlling the external stimuli. In the last two cases, the regeneration of Cu^{I} activator is controlled by external stimulation, but the rate constant of radical formation (activation) is not affected.[12k] Therefore, the polymerization stops after activator is consumed by oxidation or termination but not immediately after removing the external stimuli.

Scheme 1. ATRP equilibria in a) normal ATRP with Cu-based catalyst, b) low ppm Cu system. M: monomer.

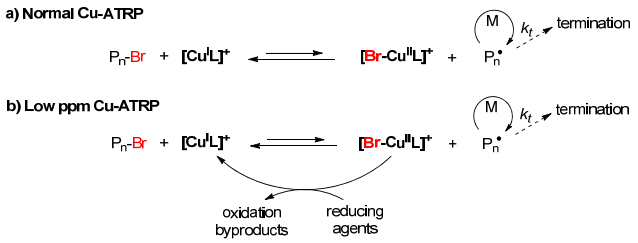

Activation rate constants for some catalysts can be enhanced by light,[13] especially for photoredox catalysts.[14] Photoredox catalysts have been extensively investigated for water splitting,[15] solar cells[16] and photodynamic therapy[17] in inorganic and materials chemistry. Recently, photoredox catalysts were also used in organic synthesis[18] and polymerization,[14,19] especially photoinduced electron transfer (PET)-RAFT.[20] Generally, photoredox catalysts behave as strong oxidants and/or reductants upon irradiation but they are poor oxidants and reductants in the ground state. Therefore, reactions with photoredox catalysts could be precisely controlled by light.

A photoinduced ATRP was successfully catalyzed by *fac*-[Ir(ppy)$_3$] (**1**, ppy = 2-pyridylphenyl, in Figure 1).[14] A simplified proposed mechanism for this process is shown in Scheme 2. Upon irradiation with visible light, excited *fac*-[Ir(ppy)$_3$]* (**1***), a very strong reductant, $E^{\ominus}_{\mathbf{1}^+/\mathbf{1}^*}$ = - 1.73 V vs. SCE, can reduce an alkyl bromide to generate an Ir^{IV} complex and an organic radical which initiates polymerization. The Ir^{IV} complex is a strong oxidant ($E^{\ominus}_{\mathbf{1}^+/\mathbf{1}}$ = 0.77 V vs. SCE), which could react with the propagating radical to provide the ground state catalyst **1** and polymer chain with a bromine at a chain end. The radical could be either oxidized to RX by a concerted atom transfer step, or oxidized to the carbocation which then recombines with bromide anion in a stepwise manner. Well-defined poly(methyl methacrylate) (PMMA, M_n = 22,900, M_w/M_n = 1.25) was obtained using low ppm amounts of **1** under visible light irradiation. This system was then extended to polymerize several acrylates[21] as well as provide three-dimensionally controlled nanostructures in a single step.[22]

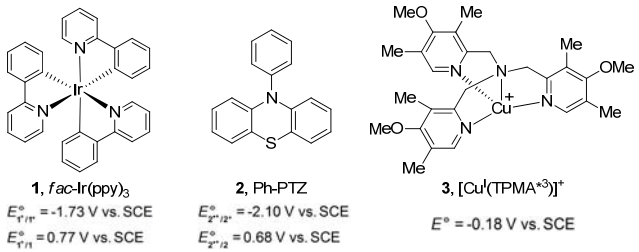

Figure 1. Structures of photoredox catalysts **1**, **2** and a traditional copper-based ATRP catalyst **3**.

A metal-free ATRP process was subsequently developed by using 10-phenylphenothiazine (**2**, Ph-PTZ, in Figure 1) as the organic-based photoredox catalyst to synthesize well-defined polymethacrylates[23] and polyacrylonitrile.[24] Analogous to **1**, Ph-PTZ **2** is also excited to form a very strong reductant Ph-PTZ* ($E^{\ominus}_{\mathbf{2}^{\bullet+}/\mathbf{2}^*}$ = - 2.10 V vs. SCE in MeCN). The oxidized radical cation Ph-PTZ$^{\bullet+}$, formed upon reaction of Ph-PTZ* with the alkyl halide, is a strong oxidant ($E^{\ominus}_{\mathbf{2}^{\bullet+}/\mathbf{2}}$ = 0.68 V vs. SCE in MeCN), able to deactivate the propagating alkyl radicals and regenerate the ground state catalyst **2**.

Scheme 2. Simplified activation/deactivation mechanism for photoredox mediated ATRP reactions. Cat = 1 or 2.

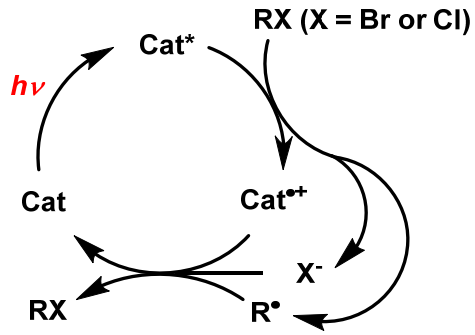

The most active Cu-based ATRP catalyst reported so far is [Cu^I(TPMA*^{3})]$^+$ (**3**, TPMA*^{3} = tris((4-methoxy-3,5-dimethylpyridin-2-yl)methyl)-amine)) which has $E^{\ominus}$ = -0.18 V vs. SCE.[25] Compared to these values, both **1** and **2** have much more negative potential values (Figure 1), indicating much greater reactivity in the activation of alkyl halides. They are so active that they can participate in both outer- and inner-sphere electron transfer (OSET and ISET) processes, while activation in Cu-based ATRP occurs *via* ISET only.[26]

The ISET *vs.* OSET dichotomy for Cu-based ATRP was previously analyzed using modified Marcus theory.[27] It was concluded that OSET should be ~ 10^9 times slower than experimentally measured ISET.[26] This is due to very high activation energy of ET to alkyl halides that are typically used in Cu-based ATRP systems. ET to these alkyl halides proceeds *via* the dissociative process with a high contribution of the breaking bond to the activation free energy of the reaction.[28] *fac*-[Ir(ppy)$_3$] **1** is a coordinatively saturated metal complex, therefore it cannot form any additional bond with the metal center, and thus the ET most likely takes place *via* an OSET.[29] In photoinduced Ph-PTZ-catalyzed metal-free ATRP system, the electron transfer (activation step) from excited Ph-PTZ* to alkyl halide most likely proceeds *via* OSET due to the tremendously negative redox potentials of the excited species ($E^{\ominus}_{\mathbf{2}^{\bullet+}/\mathbf{2}^*}$ = – 2.10 V vs. SCE for **2**, Ph-PTZ vs. $E^{\ominus}$ = – 0.18 V vs. SCE for **3**, [Cu^I(TPMA*^{3})]$^+$). It should be noted that 59 mV corresponds to one order of magnitude difference in equilibrium constants for electron transfer reactions.

The mechanism of the deactivation process also plays an important role in controlling an ATRP reaction. In atom transfer radical addition (ATRA) reactions by photoredox catalysts such as **1**, it was proposed that R$^{\bullet}$ is first oxidized to a carbocation,[30] which subsequently traps a nucleophilic halide anion to yield the product. However, in the polymerization of methyl methacrylate (MMA) and acrylonitrile (AN), the derived carbocations should be unstable and would be involved in side reactions with residual water or elimination to form short oligomers rather than polymers. No such products were observed in photoinduced metal-free ATRP, indicating that the deactivation step might not involve a carbocation as a key intermediate.

We performed a detailed mechanistic study on photoinduced metal-free ATRP to identify structure-reactivity relationships, using cyclic voltammetry (CV) and laser flash photolysis (LFP) experiments. Kinetic analysis of both activation and deactivation steps, according to Marcus theory and further developments[27] and density functional theory (DFT) calculations elucidated the following questions: 1) Does the activation step follow ISET or OSET mechanism? 2) What is the mechanism of the deactivation process during the controlled polymerization? 3) What are the key intermediates in these reactions? 4) What side reactions are involved? 5) How does this photoinduced metal-free ATRP system compare to classic Cu-catalyzed ATRP?

RESULTS AND DISCUSSION

Polymerization reactions

Polymerization of MMA with Ph-PTZ 2. The results of photoinduced metal-free ATRP of MMA with Ph-PTZ **2** under different conditions, in various solvents, under different light intensities, and in the presence of different ATRP initiators, are summarized in Table 1. The standard polymerization under conditions: [MMA]$_0$:[EBPA]$_0$:[**2**]$_0$ = 100:1:0.1, MMA/DMA = 1/1 (v/v), (EBPA: ethyl α-bromophenylacetate, DMA: dimethylacetamide), at room temperature with irradiation at 365 nm (2.1 mW/cm^2) reached 16% conversion of MMA after 4 h, yielding PMMA with M_n = 2070, and M_w/M_n = 1.50 (entry 1, Table 1) which is close to the theoretical value $M_{n,th}$ (predicted for a transferless process with a quantitative initiation). A polymerization with stronger light intensity source (4.9 mW/cm^2 at 365 nm) was faster, reaching 45 % conversion after 4 h (entry 2). The polymerization carried out in DMSO

Table 1. Selected results of metal-free ATRP of MMA under different conditions.[a]

Entry	Conditions	Time	Conv.[b]	$M_{n,th}$[c]	$M_{n,GPC}$[c]	M_w/M_n[d]
1	[MMA]:[EBPA]:[**2**] = 100:1:0.1	4 h	16%	1,800	2,070	1.50
2	[MMA]:[EBPA]:[**2**] = 100:1:0.1[e]	4 h	45%	4,700	5,440	1.44
3	[MMA]:[EBPA]:[**2**] = 100:1:0.1[f]	6 h	12%	1,400	2,500	1.98
4	[MMA]:[EBPA]:[**2**] = 100:1:0.1[g]	20 h	9%	1,100	1,120	1.78
5	[MMA]:[EBiB]:[**2**] = 100:1:0.1	4 h	20%	2,200	3,840	1.79
6	[MMA]:[EClPA]:[**2**] = 100:1:0.1[e]	4 h	55%	5,700	16,000	3.44
7	[MMA]:[EBPA]:[**2**] = 100:1:0	4 h	27%	2,900	28,700	2.25
8	[MMA]:[EClPA]:[**2**] = 100:1:0[e]	4 h	15%	1,700	17,900	2.02
9	[MMA]:[EClPA]:[**2**]:[TBABr] = 100:1:0.1:1[e]	4 h	79%	8,100	10,800	2.47

[a] Reaction conditions: MMA/DMA = 1/1 (v/v), under room temperature irradiation by 2.1 mW/cm^2, 365 nm. [b] Determined by ^{1}H NMR. [c] Calculated based on conversion obtained by ^{1}H NMR (i.e. $M_{n,th} = M_{EBPA} + 100 \times \text{conversion} \times M_{MMA}$). [d] Determined by GPC in THF, based on linear PMMA as calibration standards. [e] With 4.9 mW/cm^2, 365 nm irradiation. [f] In DMSO. [g] In MeCN.

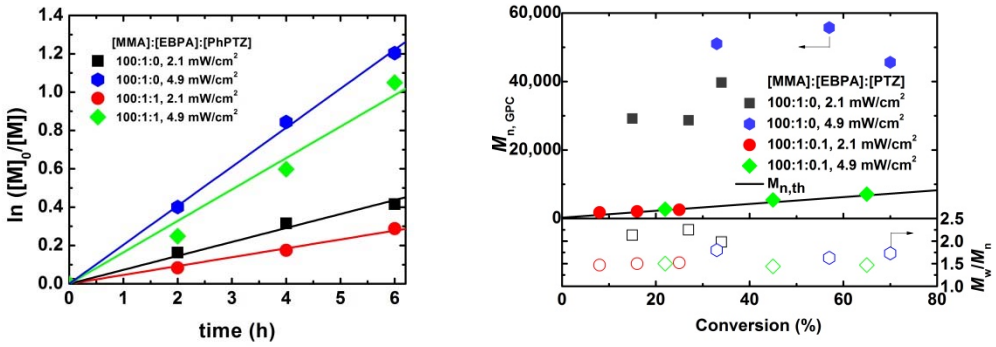

Figure 2. a) Left, semilogarithmic kinetic plots of polymerization of MMA with or without **2**; b) right, number-average molecular weight (M_n, filled symbols), and dispersity (M_w/M_n, open symbols) versus conversion.

resulted in a polymer with M_n higher than $M_{n,th}$ and with a broader molecular weight distribution (M_w/M_n = 1.98, entry 3) than the reaction in DMA, indicating limited initiation efficiency. The reaction in MeCN reached only 9% conversion after 20 h (entry 4), showing a much slower polymerization than in DMA and DMSO. With ethyl α-bromoisobutyrate (EBiB) as ATRP initiator instead of EBPA, the M_n = 3840 of PMMA was higher than $M_{n,th}$ with broader distribution (M_w/M_n = 1.79, entry 5). Indeed, activation of EBiB in ATRP is slower than activation of PMMA-Br, due to the penultimate unit effect.[31] The polymerization using ethyl α-chlorophenylacetate (EClPA) was not controlled at all, resulting in 55% conversion after 4 h with the formation of a polymer with bimodal distribution M_n = 16000, M_w/M_n = 3.44, (entry 6), indicating that a chloride-based initiator was not suitable in this photoinduced metal-free system.

Background reactions. The activation step should involve the reaction between excited state of metal-free photoredox catalyst and alkyl bromide, but under strong irradiation, the radical could also be potentially formed by homolytic cleavage of the C-Br bond in a conventional ATRP initiator or the polymer-Br chain end.[32] Polymerizations of MMA were conducted with EBPA both in the absence and presence of Ph-PTZ **2** under the following conditions: $[MMA]_0:[EBPA]_0:[\mathbf{2}]_0$ = 100:1:0 or 100:1:0.1, MMA/DMA = 1/1 (v/v), and irradiation with 365 nm at 2.1 or 4.9 mW/cm^2. Polymerization of MMA without **2** provided PMMA with much higher M_n than the theoretical value and M_w/M_n values as high as 2.2 (Table 1, entry 7 and Figure 2b), suggesting an uncontrolled free radical polymerization. These reactions also provide a clear indication that a radical could be formed from EBPA under irradiation conditions. The radical generated from EBPA could initiate the polymerization before it terminates or abstracts the bromine atom from a dormant species, P_n-Br. Therefore, EBPA could act as both polymerization initiator and transfer agent in this photomediated process.

The rates of polymerization with **2** under both irradiation conditions were slightly slower than the one without **2** (Figure 2a), indicating that the concentration of radicals was decreased and a radical deactivation process was involved in the presence of **2**. The metal-free ATRP of MMA with **2** gave PMMA with predictable M_n, growing with conversion and low dispersity, suggesting that the process is well controlled (Table 1, entries 1 and 2).

Similarly, the background reaction for polymerization of MMA with EClPA in the absence of **2** reached only 15% conversion after 4 h of irradiation with 365 nm at 4.9 mW/cm^2, providing PMMA with M_n = 17900, and M_w/M_n = 2.02 (entry 8, Table 1). However, the same reaction with **2** was much faster (entry 8 vs. 6, Table 1, 15% vs. 55% conversion at 4 h), though with the same poor control, indicating that Ph-PTZ catalyzed system is efficient to activate alkyl chloride but inefficient to deactivate the propagating radicals.

Salt effects. As in metal-catalyzed ATRP, one possible deactivation mechanism is the transfer of a halogen atom from the radical cation-anion ion pair $Cat^{\bullet+}X^-$ (X = Br or Cl) formed in the activation step to the propagating radical (eq. 1). In a polar

solvent such as DMA, the ion pair would dissociate to the free radical cation ($Cat^{\bullet+}$) and a halide anion (Br^- or Cl^-) and could reach an equilibrium state. Therefore, if deactivation occurs according to eq. 1, the overall rate of polymerization and control over molecular weight distribution would be strongly influenced by the dissociation equilibrium $Cat^{\bullet+}X^- = Cat^{\bullet+} + X^-$, which can be shifted to the left if a large excess of halide ions is added. Additionally, it must be noted that halide anions, whether linked to $Cat^{\bullet+}$ or free in solution, are a fundamental reagent of the deactivation step. Therefore, excess tetra-*n*-butylammonium bromide (TBABr) was added to improve deactivation in the polymerization of MMA when using Ph-PTZ **2** as a catalyst. However, the polymerization of MMA with added TBABr under reaction conditions $[MMA]_0:[EBPA]_0:[\mathbf{2}]_0:[TBABr]_0 = 100:1:0.1:x$, x = 0.2, 1 or 2, 50% DMA, irradiation with 365 nm, did not give any observable difference in polymerization rates and dispersities (see Figure S5).

$$Cat^{\bullet+}X^- + R^{\bullet} \longrightarrow Cat + RX \quad (1)$$

On the other hand, when an excess TBABr was added to the reaction using EClPA, the M_n (10,800) of obtained PMMA was close to the theoretical value ($M_{n,th}$ = 8,100), although the dispersity was still high (M_w/M_n = 2.47, entry 9, Table 1). The polymerization with EClPA and TBABr showed better deactivation of the growing chains, indicating that deactivation was more efficient in the presence of bromide ions.

Polymerization with different catalysts. The set of compounds shown in Figure 3 was chosen to study the effect of key structural features on their properties and reactivity. Compounds **2** and **4-7** are *N*-aryl phenothiazine derivatives; they were synthesized from phenothiazine **9** and corresponding aryl halides using Buchwald amination.[33] 10-Methylphenothiazine **8** and **9** are commercially available. The reaction of 2,3-dihydroxynaphthalene and 2-aminothiophenol provided benzo[*b*]phenothiazine,[34] which subsequently reacted with chlorobenzene under Buchwald amination, yielding phenyl benzo[*b*]phenothiazine **10**. 9-Phenylcarbazole **11** and thianthrene **12** were selected due to the structural similarity to phenothiazine, and compounds **13** and **14** were selected due to photosensitivities.[35]

All the catalysts shown in Figure 3 were investigated for photoinduced metal-free ATRP of MMA with EBPA as initiator under standard conditions. The results are summarized in Table 2 and Figures 4 and S10. The reaction conditions were $[MMA]_0:[EBPA]_0:[Cat]_0$ = 100:1:0.1, in MMA/DMA = 1/1 (v/v), at room temperature with irradiation of 365 nm at 2.1 mW/cm^2. The reactions with all phenothiazine-based compounds, **2** and **4-10,** were all slower than the background reaction, indicating that some deactivation was involved. All N-aryl phenothiazines **2**, **4-7** and benzo[*b*]phenothiazine **10** under photoinduced metal-free conditions provided well-defined PMMA with predetermined M_n and dispersities $Đ$ = 1.4-1.5 (entries 2-4 and 6, Table 2). The metal-free ATRP with catalysts **8** (Me-PTZ) and **9** (H-PTZ) only provided limited control. The obtained M_n were close to the theoretical values at low conversion of MMA (<30 %), but they became significantly higher at higher conversion (entry 5, Table 2). This observation indicates that both **8** and **9** decomposed during the later stage of the reaction and could not deactivate the radicals, as previously suggested.[23]

The polymerizations with **11** (Ph-CBZ), **12** (TH), **13** (TIPS-AN) and **14** ((CBZ-Ph)$_2$) provided faster reactions than the background reaction (entries 7 and 8 vs. entry 1, Table 2), indicating that these catalysts efficiently activated the C-Br bond but could not deactivate the propagating radical efficiently. This is further supported by the evidence that the M_n of synthesized PMMA using these catalysts was always much higher than theoretical M_n (Figures 4b and 10b).

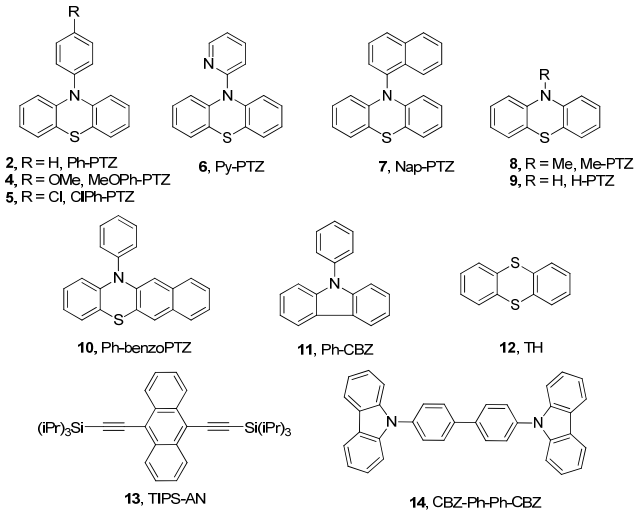

Figure 3. The structures of catalysts studied in metal-free ATRP.

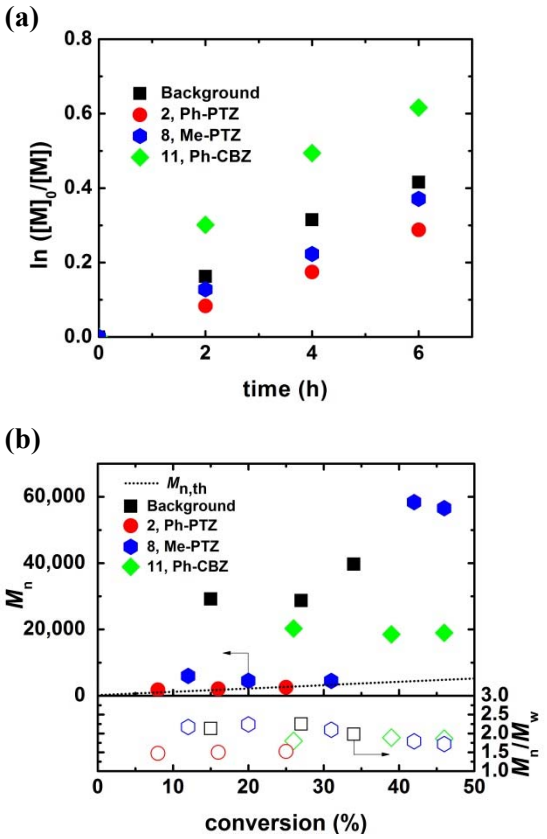

Figure 4. a) Semilogarithmic kinetic plots of polymerization of MMA with catalysts **2**, **8** and **11**, conditions: $[MMA]_0:[EBPA]_0:[Cat]_0$ = 100:1:0.1, in MMA/DMA = 1/1 (v/v), at room temperature with irradiation of 365 nm (2.1 mW/cm^2); b) number-average molecular weight (M_n, filled symbols), and dispersity (M_w/M_n, open symbols) versus conversion; black dot line: linear fit for theoretical molecular weight.

Table 2. Selected results of metal-free ATRP of MMA with different catalysts.[a]

Entry	Catalyst	Time	Conv.[b]	$M_{n,th}$[c]	$M_{n,GPC}$[c]	M_w/M_n[d]
1	-	4 h	27%	2,900	28,700	2.25
2	**2**, Ph-PTZ	4 h	16%	1,800	2,070	1.50
3	**5**, Cl-Ph-PTZ	4 h	11%	1,300	1,580	1.48
4	**7**, Nap-PTZ	4 h	10%	1,200	1,600	1.40
5	**8**, Me-PTZ	4 h	20%	2,200	4,520	2.24
		8 h	42%	4,400	58,400	1.79
6	**10**, Ph-benzoPTZ	4 h	9%	1,100	1,670	1.47
7	**11**, Ph-CBZ	4 h	39%	4,100	18,500	1.89
8	**13**, TIPS-AN	4 h	29%	3,100	51,550	2.56

[a] Reaction conditions: $[MMA]_0:[EBPA]_0:[Cat]_0$ = 100:1:0.1, in MMA/DMA = 1/1 (v/v), at room temperature with irradiation of 365 nm (2.1 mW/cm^2). [b] Determined by ^{1}H NMR. [c] Calculated based on conversion obtained by ^{1}H NMR (i.e. $M_{n,th} = M_{EBPA} + 100 \times \text{conversion} \times M_{MMA}$). [d] Determined by GPC in THF, based on linear PMMA as calibration standards.

Since the background reaction using EBPA as initiator was a fast process, it was not possible to determine whether all catalysts were involved in the activation step. Therefore, EBiB was used as the initiator rather than EBPA under metal-free ATRP conditions. All the polymerizations with any of the catalysts shown in Figure 3 were faster than the background reaction using only EBiB, strongly indicating that all the catalysts efficiently photoactivated alkyl halides (Figures 5 and S11).

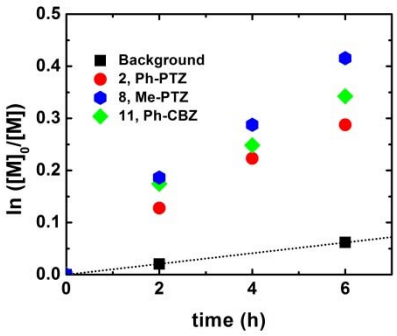

Figure 5. Semilogarithmic kinetic plots of polymerization of MMA with catalysts **2**, **8** and **11**, conditions: $[MMA]_0:[EBiB]_0:[Cat]_0$ = 100:1:0.1, in MMA/DMA = 1/1 (v/v), at room temperature with irradiation of 365 nm (2.1 mW/cm^2); black dot line: linear fit for background polymerization.

Characterizations and Properties of Catalysts

Redox potentials. Various catalyst properties were determined to better understand their different reactivities. The results are summarized in Table 3. Cyclic voltammetry (CV) was used to measure the oxidation potentials of the catalysts and to assess the stability of their radical cations ($Cat^{\bullet+}$). All CVs were recorded in DMA in the presence of 0.1 M Et_4NClO_4 and some examples are reported in Figure 6. Within the electrochemical potential window of the solvent, all compounds, except **13**, could be oxidized to form a radical cation ($Cat = Cat^{\bullet+} + e^-$). The reversibility of the voltammetric pattern is a direct indication of the stability of the radical cations. All substituted phenothiazines (**2**, **4-8**, **10**) showed a reversible oxidation wave (Figure 6a), indicating that the electrogenerated radical cation was a stable species (lifetime ≥ 1 min). The CV of unsubstituted phenothiazine **9** had limited chemical reversibility: the radical cation quickly decomposed to form a product that was reduced at a lower potential (Figure 6b). From cyclic voltammetry conducted at different scan rates, a lifetime of the order of 10 s was estimated for the radical cation **9**$^{\bullet+}$ (see Figure S9). Also **12** showed a similar behavior with a faster decay rate, with a lifetime < 5 ms. Other tested carbazole derivatives (**11** and **14**) exhibited an irreversible oxidation peak, indicating that their specific radical cations were not stable in DMA.

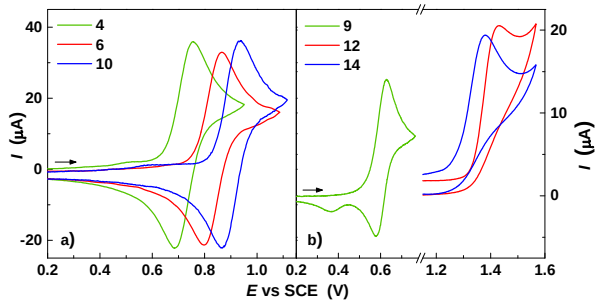

Figure 6. Selected cyclic voltammograms for compounds characterized by (a) reversible and (b) partially reversible or irreversible oxidation, $C = 2\times10^{-3}$ M, in DMA + 0.1 M Et_4NClO_4 at 25 °C. (a) v = 0.2 V s^{-1}; (b) v = 0.05 V s^{-1}.

A stable radical cation is necessary for the efficient deactivation of the growing radicals, thus only the compounds with a reversible redox behavior should efficiently control the polymerization. The experimental results confirmed this conclusion as effective deactivation was observed only for compounds with reversible redox properties. Moreover, CV analysis confirmed the limited stability of **9**$^{\bullet+}$ (H-PTZ$^{\bullet+}$, Figure 6b), which indeed could efficiently deactivate the growing radicals only at the beginning of the experiment, since a fraction of **9**$^{\bullet+}$ decomposed by side reactions leading to the progressive consumption of the catalyst. Therefore, cyclic voltammetry was a reliable technique that allowed rapid screening of the analyzed photoactive molecules as candidates for radical deactivation and control of photoATRP experiments. CV experiments also demonstrated that stable radical cations $Cat^{\bullet+}$ should be involved in the deactivation reaction mechanism.

For the compounds exhibiting a reversible redox behavior, the oxidation potential of the catalyst in the excited state ($E^{\ominus}_{Cat^{\bullet+}/Cat^*}$) could be estimated from the excitation energy of the photocatalysts ($E_{h\nu}$), according to the following equation:[16]

$$E^{\ominus}_{Cat^{\bullet+}/Cat^*} = E^{\ominus}_{Cat^{\bullet+}/Cat} - E_{h\nu} = E^{\ominus}_{Cat^{\bullet+}/Cat} - \frac{hc}{\lambda_{max}} \quad (2)$$

Table 3. Characterizations and reactivities of catalysts studied in metal-free ATRP in DMA.

Catalyst	$E^{\ominus}_{Cat^{\bullet+}/Cat}$ (V vs. SCE)	λ_{max} (nm)	$E^{\ominus}_{Cat^{\bullet+}/Cat^{*}}$ (V vs. SCE)[a]	Lifetime τ_0 (ns)[b]	CV reversibility	Activation[c]	Deactivation[d]
2, Ph-PTZ	0.815[e]	445	-1.97	4.5	+	+	+
4, MeOPh-PTZ	0.797	445	-1.99	6.0	+	+	+
5, ClPh-PTZ	0.830	445	-1.96	3.0	+	+	+
6, Py-PTZ	0.903	510	-1.53	7.4	+	+	+
7, Nap-PTZ	0.833	405	-2.23	7.6	+	+	+
8, Me-PTZ	0.826	445	-1.97	2.3	+	+	+/–
9, H-PTZ	0.606	450	-2.15	2.1	+/–	+	+/–
10, Ph-benzoPTZ	0.902	440	-1.92	12.9	+	+	+
11, Ph-CBZ	1.423[f]	375	-1.91	4.7	–	+	–
12, TH	1.393[g]	445	-1.36	4.9	–	+	–
13, TIPS-AN	>1.5[h]	445	-	2.1	–	+	–
14, (CBZ-Ph-)$_2$	1.392[f]	410	-	3.4	–	+	–

[a] From eq. 2. [b] Lifetime of the excited catalyst, Cat*. [c] Activation based on whether polymerization was faster than the background reaction with EBiB as ATRP initiator (cf. Figures 5 and S11). [d] Deactivation evaluation based on whether $M_{n,GPC}$ was close to $M_{n,th}$ (cf. Figures 4b and 10b). [e] For comparison, values in MeCN are $E^{\ominus}_{2^{\bullet+}/2} = 0.68$ V vs. SCE and $E^{\ominus}_{2^{\bullet+}/2^{*}} = -2.10$ V vs. SCE.[23] [f] Potential of the anodic peak at $v = 0.2$ V s^{-1}. [g] $E^{\ominus}_{Cat^{\bullet+}/Cat}$ was estimated at high scan rates ($v > 10$ V s^{-1}), where partial reversibility in CV could be achieved (Figure S9). [h] No oxidation wave was observed inside the potential range of DMA.

where h is the Planck constant, c is the speed of light, λ_{max} is the wavelength of maximum emission intensity of excited state and $E^{\ominus}_{Cat^{\bullet+}/Cat}$ is the standard reduction potential of $Cat^{\bullet+}$ in the ground state. $E^{\ominus}_{Cat^{\bullet+}/Cat}$ was obtained from cyclic voltammetry as the half sum of anodic (E_{pa}) and cathodic (E_{pc}) peak potentials, $E^{\ominus}_{Cat^{\bullet+}/Cat} \approx E_{1/2} = (E_{pa} + E_{pc})/2$.

LFP Measurements. Laser flash photolysis (LFP) experiments were used to measure the lifetime of the excited states of the catalysts **2**, **4**-**14**. All of them are near or below 10 ns (Table 3);[36] they are much short-lived, at least hundreds of ns, than the excited states of transition-metal based photoredox catalysts. For example, the lifetime of the excited state of **1** is 1,900 ns.[29]

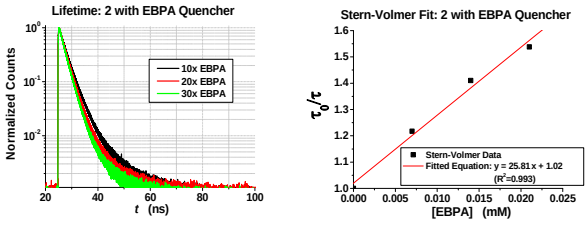

Figure 7. a) Left, decay of the excited state of **2** with increasing concentrations of EBPA; b) right, results of Stern-Volmer treatment.

The rate constant for the reaction between an excited catalyst and EBPA, a conventional ATRP initiator, was then measured. Ph-PTZ **2** was excited upon irradiation and allowed to react with increasing concentrations of EBPA. Figure 7 summarizes the results of these experiments. The rate constant for the reaction of the excited state of **2** with EBPA was determined according to the Stern−Volmer equation (eq 3):[18f]

$$\frac{1}{\tau} = \frac{1}{\tau_0} + k_{act}[Q] \quad (3)$$

where k_{act} is the rate constant, $[Q]$ is the concentration of the quencher and τ_0 is the lifetime of the excited state of **2** in the absence of a quencher. A plot of the reciprocal of the lifetime of the excited state against the concentration of EBPA provided the rate constant $k_{act} = 5.7 \times 10^9$ M^{-1}s^{-1}. The quenching experiment strongly supports the fact that the excited state of **2** is a strong reductant and efficiently reduces the ATRP initiator.

Kinetic Evaluation of the Activation Mechanism by Modified Marcus Theory

The strongly negative values for $E^{\ominus}_{Cat^{\bullet+}/Cat^{*}}$ suggested the viability of an OSET (eq. 4). This reaction involves a concerted dissociative electron transfer (DET) to RX, as consolidated in the literature for the reductive cleavage of alkyl halides.[28,37] Therefore, assessment of ET kinetics cannot be made by a straight forward application of the well-known Marcus theory for electron-transfer processes.[27a] A modified model of Marcus theory, developed by Savéant,[27b-d] is available and is currently used to analyze the dynamics of DET processes.[37b-e,38]

$$Cat + RX \xrightarrow{k_{act}} Cat^{\bullet+} + R^{\bullet} + X^{-} \quad (4)$$

According to the DET theory,[27c] a quadratic activation-driving force relationship similar to that of Marcus theory of OSET exists also for DET processes (eq. 5).

$$\Delta G^{\ddagger} = \Delta G_0^{\ddagger}\left(1 + \frac{\Delta_r G^{\ominus}}{4\Delta G_0^{\ddagger}}\right)^2 \quad (5)$$

where $\Delta G_0^{\ddagger}$ is the intrinsic barrier of the reaction, i.e. the activation free energy when $\Delta_r G^{\ominus} = 0$. The intrinsic barrier is given by $\Delta G_0^{\ddagger} = (\lambda_o + D_{RX})/4$, where λ_o is the solvent reorganization energy and D_{RX} is the R-X bond energy. The principal difference between OSET and DET is that the intrinsic barrier of the latter mainly comes from the energy of the breaking bond. When the two fragments of DET, $R^{\bullet}$ and X^{-}, are able to give rise to ion-dipole interactions in the solvent cage, the dynamics of ET is significantly affected and eq. 5 does not correctly predict the activation free energy. The "sticky" model of DET takes into account formation of

Table 4. Activation rate constants and relevant thermodynamic parameters for reaction (4) in DMA.

Donor	RX	$E^{\ominus}_{Cat^{\bullet+}/Cat^{*}}$	$E^{\ominus}_{RX/R^{\bullet}+X^{-}}$	$\Delta_r G^{\ominus}$	$\Delta G_0^{\ddagger}$	$\Delta G^{\ddagger}$	$Z\times10^{-11}$	k_{act}	φ_{act}[b]
		V vs. SCE	V vs. SCE[a]	kcal mol^{-1}	kcal mol^{-1}	kcal mol^{-1}	M^{-1}s^{-1}	M^{-1}s^{-1}	
1*, Ir(ppy)$_3$*	MBiB	-1.73[c]	-0.52	-28.9	16.4	5.1	3.0	5.8×10^{7}	0.4
2*, Ph-PTZ*	MBiB	-1.97	-0.52	-34.6	16.5	3.7	2.9	5.8×10^{8}	1.3×10^{-3}
2*, Ph-PTZ*	EBPA	-1.97	-0.22[d]	-41.5	15.3	1.6	2.8	2.0×10^{10}	4.6×10^{-2}
2*, Ph-PTZ*	MCiB	-1.97	-0.76	-29.1	19.2	7.2	3.2	1.5×10^{6}	3.5×10^{-6}
2, Ph-PTZ	MBiB	0.82[e]	-0.52	29.6	16.5	34.5	2.7	1.0×10^{-14}	-
8*, Me-PTZ*	MBiB	-1.96	-0.52	-34.4	16.6	3.8	2.6	4.3×10^{8}	5.0×10^{-4}
11*, Ph-CBZ*	MBiB	-1.91	-0.52	-33.3	15.5	4.0	2.8	3.3×10^{8}	7.7×10^{-4}

[a] In DMF.[39] [b] Calculated from eq. 8 or 9. $C_{RX} = 5\cdot10^{-2}$ M; τ_0 from Table 3; Φ_F was determined to be roughly constant and on average 0.01 for a large set of phenothiazine derivatives,[40] therefore $\Phi_F = 0.01$ was used for **2***, **8*** and **11***; $\Phi_F = 0.40$ for **1***.[41] [c] In MeCN.[20g] [d] in DMF, calculated as in Ref. 39, using thermodynamic data from Ref. 26a. [e] $E^{\ominus}_{Cat^{\bullet+}/Cat^{-}}$.

the ion-dipole adduct by introducing the interaction energy, D_p, into eq. 5:

$$\Delta G^{\ddagger} = \Delta G_0^{\ddagger}\left(1+\frac{\Delta_r G^{\ominus} - D_p}{4\Delta G_0^{\ddagger}}\right)^2 \quad (6)$$

Although D_p is of electrostatic nature and is often very small,[37d] it decreases significantly the intrinsic barrier, now given by $\Delta G_0^{\ddagger} = [\lambda_o + \left(D_{RX}^{1/2} - D_p^{1/2}\right)^2]/4$, resulting in enhanced rate of electron transfer.

Eq. 6 was used to calculate $\Delta G^{\ddagger}$ of reaction 4 for a series of catalysts and two ATRP initiators. The activation free energy was then used to calculate the activation rate constant, k_{act}, according to eq. 7:

$$k_{ET} = k_{act} = Z\exp\left(-\frac{\Delta G^{\ddagger}}{RT}\right) \quad (7)$$

where Z is the pre-exponential factor. The results are presented in Table 4, whereas details of the calculations as well as all parameters used in eqs. 6 and 7 are reported in the Supporting Information. In the examined cases, Cat can be an organic molecule in the excited state (e. g. **2***), the same organic molecule in the ground state (**2**), or the excited state metal complex **1***. RX is methyl 2-bromoisobutyrate (MBiB), which mimics the PMMA growing chain end. The driving force for the photoinduced electron transfer ($\Delta_r G^{\ominus}$) is estimated from the standard potentials of the redox couples of the donor ($Cat^{\bullet+}$/Cat) and acceptor ($RX/R^{\bullet}+X^{-}$), $E^{\ominus}_{Cat^{\bullet+}/Cat}$ and $E^{\ominus}_{RX/R^{\bullet}+X^{-}}$, and the energy to excite the catalyst, $E_{h\nu}$, by using the Weller equation:[42]

$$\Delta_r G^{\ominus} = F(E^{\ominus}_{Cat^{\bullet+}/Cat} - E^{\ominus}_{RX/R^{\bullet}+X^{-}} - E_{h\nu}) - \frac{N_A e^2}{4\pi\varepsilon_0\varepsilon r} \quad (8)$$

where N_A is the Avogadro constant, e is the elementary charge, ε_0 is the permittivity of vacuum and ε the relative permittivity of the solvent at 25 °C. The last term is the Columbic energy experienced by the radical ion pair at distance r.

Unfortunately, not all the data required for estimating the frequency factor Z, $\Delta G_0^{\ddagger}$ and D_P in DMA are available; therefore, it was assumed that the thermodynamic data for RX reduction and bond dissociation were similar in DMF and in DMA. Also, the "sticky" interaction energy between methyl isobutyrate radical ($MiB^{\bullet}$) and Br^{-} is unknown in DMA but this interaction, for activated alkyl bromides, like MBiB, is always small in polar solvents like DMF and CH_3CN (0.24–0.50 kcal mol^{-1}).[26b] Radical–anion interactions depend on the dielectric constant, which are very similar for CH_3CN, DMF and DMA. Therefore, we considered that this contribution to the activation energy should be similar to the one reported for the methyl propionate radical ($MP^{\bullet}$) and Br^{-} in CH_3CN (0.24 kcal mol^{-1}).

All excited catalysts show high reactivity with RX with k_{act} values in the 10^6-10^{10} M^{-1}s^{-1} range. For the DET reaction between EBPA and **2***, $k_{act} = 5.7\times10^{9}$ M^{-1} s^{-1} was obtained from FLP measurements in DMA, whereas the calculated value is 2.0×10^{10} M^{-1} s^{-1}. Considering that a series of approximations had been forcefully introduced into the calculation, the agreement between experiment and theory can be considered to be satisfactory. Therefore, unlike transition-metal catalyzed ATRP which involves activation *via* an atom transfer (or ISET) mechanism, activation in photoinduced ATRP follows a concerted dissociative electron transfer mechanism (an OSET mechanism).

All the analyzed phenothiazine derivatives have redox properties that are relatively similar to each other. Table 4 shows that **2*** (Ph-PTZ*) and **8*** (Me-PTZ*) should react with MBiB with similar high rate constants (5.8×10^{8} and 4.3×10^{8} M^{-1}s^{-1}, respectively). Such values are higher than k_{act} reported for extremely active Cu-based ATRP systems (activation of tertiary RBr initiators by $[Cu^{I}Me_6TREN]^{+}$ in water[43] or DMSO[44]), and are typical of fast polymerizations that are often difficult to control.[45] Nevertheless, these values cannot be directly compared to the k_{act} of a traditional ATRP, because reactions that occur from an excited state are usually less than 100% efficient. ATRP activation by Cat* must compete with all decay pathways (radiative and non-radiative) that can bring the molecules back to their ground state. The quantum yield for a first-order reaction from a given excited state is:[46]

$$\varphi = \frac{k'}{k'+k_0}\Phi_F \cong \frac{k'}{k_0}\Phi_F \cong k'\tau_0\Phi_F \quad (9)$$

where k' is the rate constant of the first-order reaction that occurs from the excited state, Φ_F is the quantum efficiency for the formation of the excited state, k_0 is the rate constant of radiative decay, and $\tau_0 = 1/k_0$ is the lifetime of the excited state. ATRP activation can be considered a pseudo-first-order reaction, with rate constant k', if we take into account that the polymerization is living and that therefore RX concentration is

roughly constant during the reaction ($k' = k_{act}[RX]$). Therefore eq. (9) can be written as

$$\varphi_{act} = k_{act}[RX]\tau_0\Phi_F \quad (10)$$

Quantum yields for metal-free ATRP activation are reported in Table 4. For example, with $\varphi_{act} = 1.3\times10^{-3}$, only 1 out of *ca.* 10^3 molecules of **2*** survives for a sufficiently long time in the excited state to be able to activate MBiB. In other words, even if **2*** is able to react with MBiB with a rate constant of 5.8×10^8 M s^{-1}, the actual rate of activation is significantly decreased by the low lifetime τ_0 of the excited state and the fluorescence quantum efficiency Φ_F. Since the rate of activation is also the rate of formation of the deactivator, these parameters affect also the deactivation steps. In particular, deactivation can occur only if the rate of activation by Cat* is higher than the background reaction, which is the case for all analyzed compounds, as shown in Figures 5 and S11.

A further insight into the efficiency of activation (eq. 9 and 10) can indicate why the photoinduced ATRP of MMA required only 50-100 ppm of **1**, but 1000 ppm of **2**. When comparing **1*** and **2***, the former has both longer lifetime (1900 vs. 4.5 ns) and higher quantum efficiency (0.40 vs. 0.01). As shown in Table 4, **1*** can activate the RX bond much more efficiently than **2***. Therefore, a much higher portion of the Ir complex will be part of the activation/deactivation process, while under the same conditions most of **2*** will quickly decay back to the ground state, thereby being unable to participate in any activation/deactivation process.

The standard reduction potential of PMMA$^\bullet$ is expected to be similar to (or only slightly more negative than) that of MiB$^\bullet$, -0.70 V vs. SCE.[47] Moreover, the activation energy of this reaction is low, because the reduction of the radicals does not require the scission of any bond. As a result, radicals can be quickly reduced to carbanions by Cat*, with a diffusion-controlled rate constant. However, in a controlled ATRP process, like that under investigation, the concentration of R$^\bullet$ is very small, and hardly ever exceeds 10^{-6} M. Therefore, the rate of radical reduction, which is proportional to both Cat* and R$^\bullet$ concentrations, is essentially too slow to compete with other radical reactions such as propagation and deactivation back to the dormant state. The preserved chain end functionality is high, as confirmed by several successful chain extension tests.[23-24]

From Table 4, it is clear that the standard potential of the **2**$^{\bullet+}$/**2** couple in the ground state is too positive to effectively reduce RX and generate radicals. Therefore, the reaction cannot proceed in the absence of light. When the light source is switched off, activation stops almost instantly because of the very fast decay of Cat* to its ground state.

DFT Calculations of the Activation and Deactivation Mechanisms

In order to obtain further insights into the mechanisms of the activation and the deactivation processes, and to explore factors that affect the efficiency of the metal-free photoredox catalysts, DFT calculations were carried out for the reactions with selected catalysts **2** (Ph-PTZ), **8** (Me-PTZ) and **11** (Ph-CBZ).[48,49]

Activation Mechanism. The activation processes involving the reactions of excited **2***, **8***, and **11*** with MBiB and **2*** with MCiB (eq. 4, Cat = **2***, **8***, or **11***, RX = MBiB or MCiB) were examined through DFT calculations. Here, MBiB and MCiB were used as a model of the PMMA growing chain end. Geometry optimizations of the radical anions of MBiB and MCiB led to dissociation to the free MiB radical and Br^- or Cl^-. The instability of the RX radical anion confirms that ET from Cat* to RX (eq. 4) is a concerted dissociative ET process. The standard free energies obtained from DFT calculations for the dissociative ET to form R$^\bullet$ and X^- were used to estimate the activation free energies and rate constants according to the sticky model of DET (eqs. 6 and 7). Table 5 reports the computed reaction free energies and the activation free energies calculated from eq. 6. The agreement between the computed activation energies and those derived from experimental data, is not very good in some cases. This could be due to the uncertainty in the computed free energy of solvation of ions (see Supporting Information, Table S2). All reactions are highly exergonic and have low barrier for the dissociative electron transfer. This confirms that DET activation is highly likely with all three catalysts.

Table 5. Computed reaction energies, and activation free energies in the activation processes, with the excited catalysts 2*, 8*, and 11*.

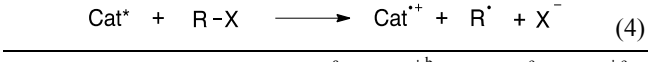

(4)

Cat	R-X	$\Delta_r G^{\circ}$ [a]	$\Delta G^{\ddagger}$ [b]	$\Delta_r G^{\circ}$ [c]	$\Delta G^{\ddagger}$ [c]
2*, Ph-PTZ	MBiB	−30.4	4.7	−34.6	3.7
2*, Ph-PTZ	MCiB	−30.9	6.8	−29.1	7.2
8*, Me-PTZ	MBiB	−32.0	4.4	−34.4	3.8
11*, Ph-CBZ	MBiB	−25.1	6.3	−33.3	4.0

[a] Reaction free energies (in kcal mol^{-1}) are computed at the M06-2X/6-311++G(3df,2p)//B3LYP/6-31G(d) level of theory. The SMD solvation model with DMF solvent was used in geometry optimizations and single point energy calculations. [b] Activation barriers of DET pathway calculated from eq. 6 using DFT-calculated reaction energies (see Supporting Information for details). [c] Calculated from eqs. 6 ($\Delta G^{\ddagger}$) and 8 ($\Delta_r G^{o}$).

Structures and stabilities of intermediates Cat$^{\bullet+}$ and Cat$^{\bullet+}$X$^-$. A key factor that determines whether the deactivation occurs through an inner-sphere or an outer-sphere ET mechanism is the structural stability of the resulting radical cation and halide anion complex **Cat**$^{\bullet+}$**X**$^-$ formed after the activation. The optimized geometries and energies of the radical cation **2**$^{\bullet+}$ and two lowest energy isomers of the **2**$^{\bullet+}$**Br**$^-$ complex are shown in Figure 8. The DFT calculations indicate that both isomers of **2**$^{\bullet+}$**Br**$^-$ have similar Gibbs free energies in solution as the dissociated radical cation **2**$^{\bullet+}$ and **Br**$^-$. Isomer **2**$^{\bullet+}$**Br**$^-$**-C** (C stands for covalent) has stronger covalent interactions between the S atom in the catalyst and the bromide anion, while the interactions between the catalyst radical cation and the bromide in isomer **2**$^{\bullet+}$**Br**$^-$**-I** (I stands for ionic) are mostly ionic. This difference is supported by the shorter S−Br distance (3.03 and 4.04 Å, respectively) and a greater S−Br Wiberg bond index (0.12 and 0.01, respectively) in **2**$^{\bullet+}$**Br**$^-$**-C** than in **2**$^{\bullet+}$**Br**$^-$**-I**. In addition, the Br atom in the covalent complex **2**$^{\bullet+}$**Br**$^-$**-C** is less negatively charged and has greater spin density than the Br in the ionic complex (Figure 8). Due to the ionic character of **2**$^{\bullet+}$**Br**$^-$**-I**, the geometry of the phenothiazine rings in the ionic complex **2**$^{\bullet+}$**Br**$^-$**-I** is almost completely planar, the same as the dissociated radical cation.[50] In contrast, the phenothiazine is bent in **2**$^{\bullet+}$**Br**$^-$**-C**, which resembles the geometry of **2** in the ground state. Nonetheless, the relative Gibbs free energies, the S-Br distances and bond orders all indicate that the interactions between the catalyst radical cation and the bromide anion

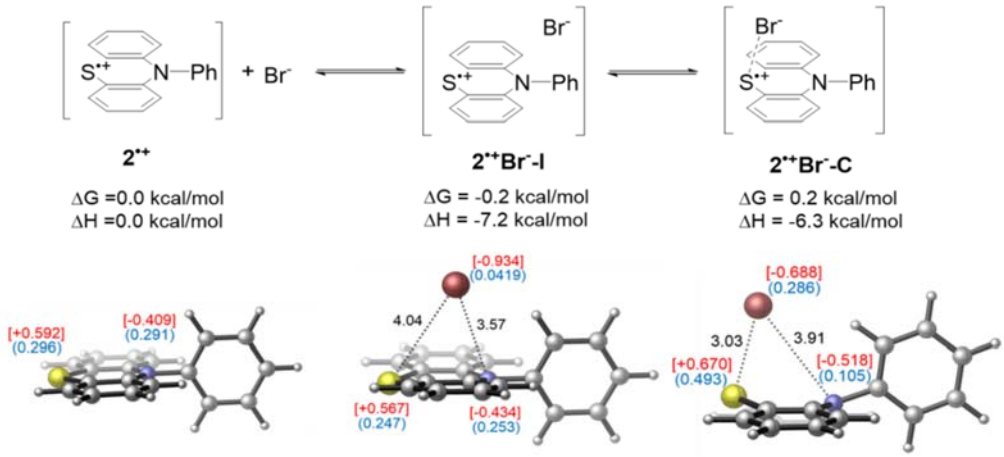

Figure 8. Optimized geometries of the radical cation $\mathbf{2}^{\bullet+}$ and the zwitterionic radical complex $\mathbf{2}^{\bullet+}\mathbf{Br}^{-}$. The bond lengths are provided in Å. NPA atomic charges of Br, S, and N atoms are shown in red in square brackets. Spin densities are shown in blue in parentheses.

Scheme 3. Possible deactivation mechanisms in photoinduced metal-free ATRP.

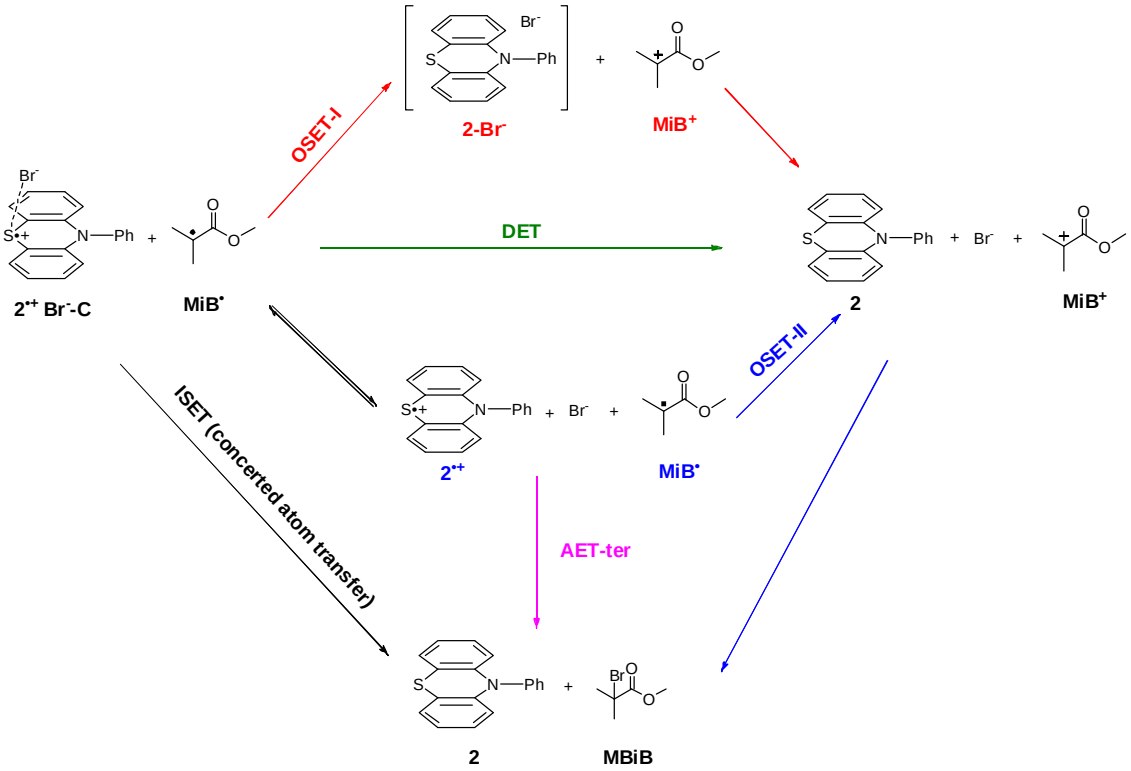

in $\mathbf{2}^{\bullet+}\mathbf{Br}^{-}$ in solution are relatively weak, and $\mathbf{2}^{\bullet+}$, $\mathbf{2}^{\bullet+}\mathbf{Br}^{-}$**-C**, and $\mathbf{2}^{\bullet+}\mathbf{Br}^{-}$**-I** may all exist in equilibrium.[51]

Similarly, calculations on other $\mathbf{Cat}^{\bullet+}\mathbf{X}^{-}$ complexes indicate that their dissociation to the separated radical cation and halide anion are all facile. The most stable isomers of $\mathbf{2}^{\bullet+}\mathbf{Cl}^{-}$, $\mathbf{8}^{\bullet+}\mathbf{Br}^{-}$, and $\mathbf{11}^{\bullet+}\mathbf{Br}^{-}$ complexes are all within ±1 kcal/mol of the separated ionic species in terms of Gibbs free energies. The optimized geometries, computed spin densities, charges, and Wiberg bond indices of these ion pair complexes are shown in Figure S12. One of the lowest energy isomers of $\mathbf{8}^{\bullet+}\mathbf{Br}^{-}$ (MePTZ$^{\bullet+}$Br^{-}) shows strong covalent interactions between S and Br atoms, similar to those in $\mathbf{2}^{\bullet+}\mathbf{Br}^{-}$**-C.** However, no isomers with clear covalent interactions between $\mathbf{Cat}^{\bullet+}$ and $\mathbf{X}^{-}$ were located for $\mathbf{11}^{\bullet+}\mathbf{Br}^{-}$ or $\mathbf{2}^{\bullet+}\mathbf{Cl}^{-}$.

Deactivation mechanisms. Since the DFT calculations have shown that both the catalyst radical cation $\mathbf{2}^{\bullet+}$ and the ion pair complex $\mathbf{2}^{\bullet+}\mathbf{Br}^{-}$ exist in solution, five possible deactivation mechanisms of the MiB$^{\bullet}$ with $\mathbf{2}^{\bullet+}$ or with 2$^{\bullet+}$Br^{-}-C[52] were evaluated (Scheme 3): (a) inner-sphere electron transfer (ISET) mechanism through a concerted Br atom transfer from $\mathbf{2}^{\bullet+}\mathbf{Br}^{-}$**-C** to MiB$^{\bullet}$ *via* transition state **TS1**; (b) dissociative electron transfer (DET) from MiB$^{\bullet}$ to $\mathbf{2}^{\bullet+}\mathbf{Br}^{-}$**-C** to form the carbocation, **2** and $\mathbf{Br}^{-}$, followed by recombination of MiB^{+} and Br^{-} to generate MBiB; (c) outer-sphere electron transfer (OSET-I) from MiB$^{\bullet}$ to $\mathbf{2}^{\bullet+}\mathbf{Br}^{-}$**-C** to form an anionic **2** $\mathbf{Br}^{-}$ complex and MiB^{+}, followed by dissociation to the catalyst **2** and $\mathbf{Br}^{-}$, and counteriaons recombination; (d) outer-sphere electron transfer from MiB$^{\bullet}$ to the dissociated radical cation $\mathbf{2}^{\bullet+}$ (OSET-II); and (e) associative electron transfer from $\mathbf{2}^{\bullet+}$ to MiB$^{\bullet}$ and $\mathbf{Br}^{-}$ to form the ground-state catalyst **2** and MBiB, involving a termolecular encounter (AET-ter). ISET and AET-ter pathways produce RX without the formation of any intermediate, while all other ET pathways (DET, OSET-I, and OSET-II) generate the R^{+} cation, which then rapidly

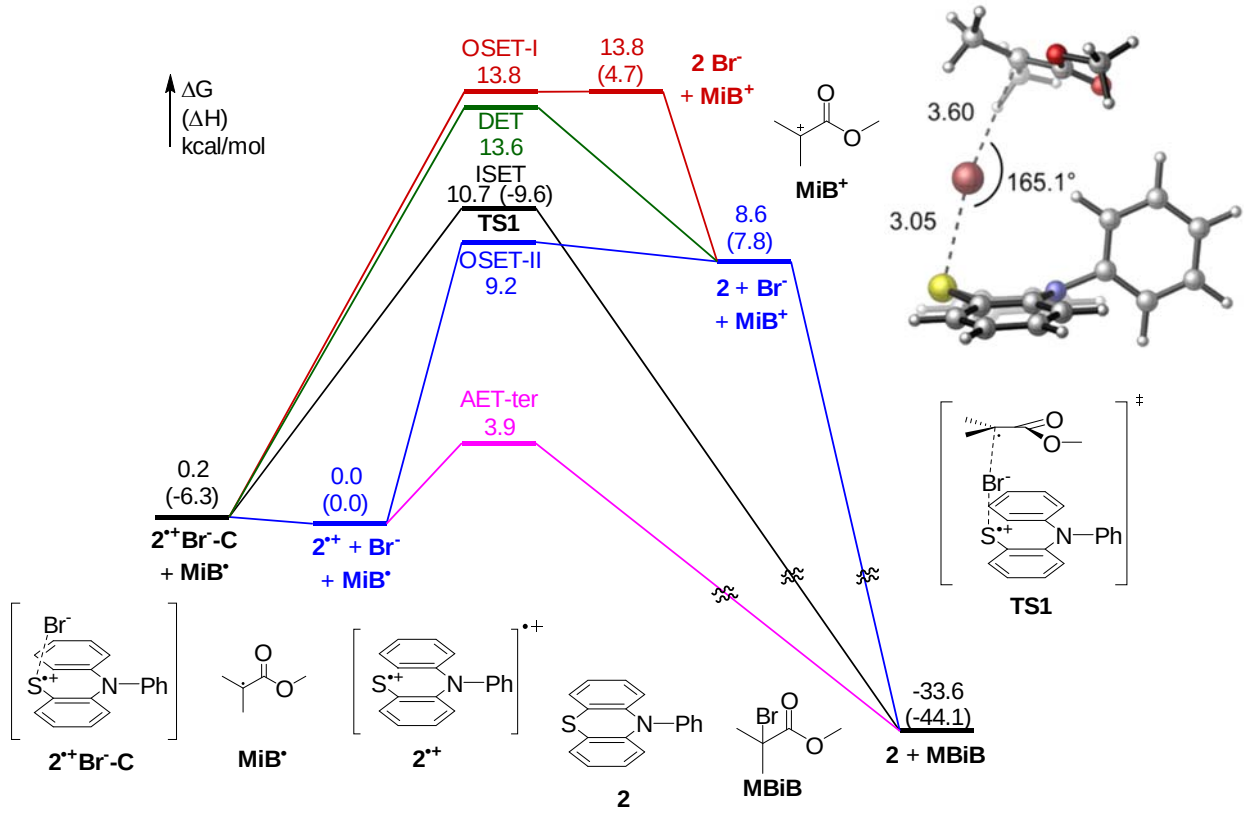

Figure 9. Computed reaction energy profiles for the reaction of **2**•⁺**Br**⁻**-C** with MiB•. Magenta: associative electron transfer involving a termolecular encounter (AET-ter). Black: inner-sphere electron transfer (ISET) (*i.e.* concerted atom transfer); Green: dissociative electron transfer from MiB• to **2**•⁺**Br**⁻**-C** (DET); Red: stepwise outer-sphere electron transfer from MiB• to **2**•⁺**Br**⁻**-C** to form **2** **Br**⁻ (OSET-I); Blue: outer-sphere electron transfer from MiB• to the dissociated radical cation **2**•⁺ (OSET-II). Activation free energies in the OSET pathways are calculated using the Marcus theory.

recombines with the halide anion to form RX. The transition state for the concerted Br atom transfer (ISET) was optimized with DFT calculations. The barriers for the outer-sphere electron transfer pathways (OSET-I, OSET-II) were calculated using the Marcus theory, whereas the activation free energy of the DET pathway was calculated by eq. 6. The AET-ter pathway (eq 11) is the exact reverse process of DET of the activation step with the catalyst at the ground state (eq 4).[53]

$$Cat^{\bullet+} + R^{\bullet} + X^{-} \xrightarrow{k_{AET\text{-}ter}} Cat + RX \qquad (11)$$

Since the intrinsic barrier is defined as the activation free energy at zero driving force, reactions 4 and 11 have the same $\Delta G_0^{\ddagger}$ value. $\Delta G_0^{\ddagger}$ and $\Delta G^{\ddagger}$ were already calculated for Ph-PTZ + MBiB (Table 4). Nevertheless we recalculated $\Delta G^{\ddagger}$ using DFT data for a better comparison of this reaction route with the other reaction pathways for which only DFT data are available. The activation free energy can then be calculated by eq. 6. The computed reaction energy profiles of the five pathways are summarized in Figure 9 (detailed calculations in the Supporting Information).

The ISET pathway requires 10.5 kcal/mol of activation free energy with respect to the ion pair complex **2**•⁺**Br**⁻**-C**. The optimized geometry of the ISET transition state (**TS1**) is shown in Figure 9. Among the other four outer-sphere electron transfer pathways, AET-ter pathway of radical cation **2**•⁺, MiB• and Br⁻ forming **2** and MBiB has the lowest activation energy, 3.9 kcal/mol (see the Supporting Information for detailed calculations). The electron transfer from MiB• to the dissociated radical cation **2**•⁺ (OSET-II) requires 9.2 kcal/mol of activation free energy, which is close to the activation energy of ISET pathway (10.5 kcal/mol). The other two reaction pathways, OSET-I and DET, have higher barriers of 13.6 and 13.4 kcal/mol, respectively.

These calculations suggest AET-ter to be the most favored pathway. Additionally, some experimental observations are in contrast with OSET-I, OSET-II and DET. First, the reaction of **2** with EClPA (alkyl chloride) was not as controlled as the reaction between **2** and EBPA (alkyl bromide). The effects of the halide (better control with RBr than RCl) rule out the possibility of OSET-II, which should not be affected by the nature of X⁻. Also, the lack of oligomer formation during the polymerization provides further evidence against the formation of MiB⁺, thus ruling out not only OSET-II pathway but also DET and OSET-I pathways.

Computed Barriers for Deactivation Processes with Different Catalysts. The computed activation energies of deactivation reactions with different catalysts are summarized in Table 6. In reactions with MBiB, the computed $\Delta G^{\ddagger}$ values are only minimally affected when switching the catalyst from Ph-PTZ **2** to Me-PTZ **8** (entries 1 and 3). However, catalyst Me-PTZ **8** did not perform as well as catalyst **2,** probably due to the slow decomposition of **8**•⁺ (*vide supra*).[54] In the reaction with catalyst Ph-CBZ **11** (entry 4), all five possible pathways have much lower $\Delta G^{\ddagger}$ than the corresponding pathways with **2** and **8,** due to the greater oxidizing power of **11**•⁺ compared to **2**•⁺ and **8**•⁺. However, **11** is a very inefficient deactivator in the polymerization of MMA (cf. entry 7, Table 2). The poor performance of **11** is due to the instability of the radical cation **11**•⁺ shown by CV experiments. In fact, CV of **11** has shown an irreversible response even at high scan rates indicating that

Table 6. Computed activation energies for possible deactivation pathways in metal-free ATRP with photoredox catalysts 2, 8, and 11.

Entry	catalyst	initiator	activation energy for deactivation pathways $\Delta G^{\ddagger}$ ($\Delta H^{\ddagger}$) kcal/mol				
			ISET[a]	AET-ter[b]	DET[a]	OSET-I[a]	OSET-II[b]
1	**2**, Ph-PTZ	MBiB	10.5 (−3.3)	3.9	13.4	13.6	9.2
2	**2**, Ph-PTZ	MCiB	12.5 (−2.4)	6.1	16.5	11.2	9.2
3	**8**, Me-PTZ	MBiB	9.0 (−2.6)	3.7	13.2	11.5	8.3
4	**11**, Ph-CBZ	MBiB	8.3 (−3.5)	1.0	2.5	2.0	0.8

[a] Activation energies with respect to the ion pair complex $\mathbf{Cat^{\bullet+}X^-}$; [b] Activation energies with respect to separated ions $\mathbf{Cat^{\bullet+}}$ and $\mathbf{X^-}$, which energies are within 1 kcal/mol of the ion pair complex.

11$^{\bullet+}$ has a very short lifetime (*vide supra*). Computational results indicate that the homolytic cleavage of **11**$^{\bullet+}$**Br**$^-$ to form ground state **11** and a Br radical is exergonic by -1.5 kcal/mol (Scheme 4). In contrast, the homolytic dissociation of other $\mathbf{Cat^{\bullet+}X^-}$ complexes to form free halogen radical is much more unfavorable, and requires 14.0 kcal/mol, 13.8 kcal/mol, and 30.8 kcal/mol for **2**$^{\bullet+}$**Br**$^-$, **8**$^{\bullet+}$**Br**$^-$, and **2**$^{\bullet+}$**Cl**$^-$, respectively.

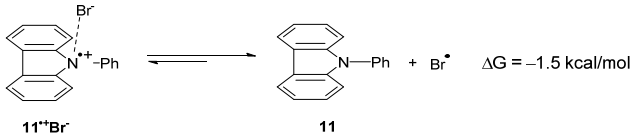

Scheme 4. Homolytic cleavage of the **11**$^{\bullet+}$**Br**$^-$ complex indicates the instability of **11**$^{\bullet+}$.

The effects of halides on the barriers of ISET and all other four deactivation pathways were then explored. When MCiB is used in place of MBiB as the initiator in the reaction with catalyst **2** (entry 2, Table 6), the barriers of the ISET, AET-ter and DET pathways increase, whereas that of OSET-I decreases. As expected, the halide has no effect on the barrier of the OSET-II pathway. While the most preferred pathway with MCiB is still AET-ter, the activation free energy is 2.2 kcal/mol higher than the reaction with MBiB.

In summary, the computed activation energies indicate that the AET-ter pathway is preferred in the deactivation process. A combination of more effective catalysts and initiator, such as **2** and **8** with MBiB (entries 1 and 3) leads to low barriers for the AET-ter pathway. The performance of catalyst **11** is impeded by the instability of both radical cation **11**$^{\bullet+}$ and complex **11**$^{\bullet+}$**Br**$^-$ that can readily dissociate to form a free bromine radical. The poor control of polymerization of MMA with alkyl chloride as ATRP initiator provides a further support for the AET-ter deactivation mechanism. With **2** as catalyst, $\Delta G^{\ddagger}$ of AET-ter increases by 2.2 kcal/mol when Cl^- is used in place of Br^-. This will result in a considerable lowering of the deactivation rate, which might not be able to outrun radical-radical termination reactions (*vide infra*).

Comparison of Rates of All Deactivation Pathways

In a controlled radical polymerization, the deactivation reaction should be faster than radical-radical termination to maintain the living character. Therefore, the rate constants and reaction rates for different deactivation pathways were calculated for catalyst **2**, and the results are summarized in Table 7. The rate of radical termination could be obtained from $R_t = k_t[R^{\bullet}]^2$, where k_t is the rate constant of radical-radical termination and [R$^{\bullet}$] is the concentration of the propagating radical. [R$^{\bullet}$] ≈ 4.6 ×10^{-8} M could be estimated from $k_p^{app} = k_p[R^{\bullet}]$, where k_p^{app} , the apparent rate constant of propagation, was obtained from the polymerization of MMA with **2** under 4.9 mW/cm^2 irradiation (Figure 2).

For a termolecular reaction pathway AET-ter, the frequency factor Z_{ter} is calculated following Tolman's approach:[55]

$$Z_{ter} = N_A^2 8\pi^2 \left(\frac{2RT}{\pi}\right)^{1/2} \left[\left(\frac{m_A + m_B}{m_A m_B}\right)^{1/2} + \left(\frac{m_B + m_C}{m_B m_C}\right)^{1/2}\right] d_{A\leftrightarrow B}^2 d_{B\leftrightarrow C}^2 \delta \quad (12)$$

where A, B and C are the three species involved in the reaction, d is the distance between the centers of the spheres equivalent to the subscript particles, and δ is the distance between the two first spheres when hit by the third. Usually δ is taken to be between 0.3 Å[53] and 1 Å.[55c] The smaller value of 0.3 Å was used to avoid overestimating Z_{TER}. The hard sphere diameters of the species involved in the reaction were estimated from their computed volumes or taken from the literature (see Supporting Information). Then, using $\Delta G^{\ddagger}_{AET\text{-}ter}$ = 3.9 kcal/mol (Table 6), the rate constant was calculated from eq. 13 as $k_{AET\text{-}ter} = 4.6\times10^7$ M^{-2} s^{-1}. This deactivation rate constant is as high as or even higher than k_{deact} in typical Cu-based ATRP.[56]

$$k_{AET\text{-}ter} = Z_{ter} e^{\frac{-\Delta G^{\ddagger}_{AET\text{-}ter}}{RT}} \quad (13)$$

The rate of termolecular deactivation is given by:

$$R_{AET\text{-}ter} = k_{AET\text{-}ter}[2^{\bullet+}][Br^-][R^{\bullet}] \quad (14)$$

However, both **2**$^{\bullet+}$ and Br^- concentration need to be estimated. Considering around 10% of termination, [Br^-] should be *ca.* 5 mM. Moreover, the CV registered during a metal-free ATRP confirmed that around 5 mM of Br^- was generated after a few hours (Figure S14). The radical cation **2**$^{\bullet+}$ could not be directly detected during the electrochemical measurements, and it slowly decomposed by the reaction with Br^-.[54] Therefore, a low value of 5×10^{-4} M was chosen for the concentration of **2**$^{\bullet+}$. Using these concentrations together with [R$^{\bullet}$] ≈ 4.6 ×10^{-8} M gives $R_{AET\text{-}ter} = 5.3\times10^{-6}$ M s^{-1}.

A similar approach was used to calculate the rate constants and rates of all other deactivation pathways (see the Supporting Information for the detailed calculations). Although the concentration of **2**$^{\bullet+}$ has a high uncertainty, the ratio of deactivation rates is independent of [**2**$^{\bullet+}$] and [**R**$^{\bullet}$]. To single out the effective deactivation pathway, the rate of all deactivation reactions must be first compared to R_t and then to each other. R/R_t values calculated for all deactivation pathways are reported in Table 7 (last column). ISET, DET and OSET-I are to be discarded as possible deactivation pathways as they are at least 2 orders of magnitude slower than termination. The rate of OSET-II is comparable with R_t, but clearly this deactivation pathway cannot provide good control. This leaves AET-ter,

Table 7. Rate constants and rates of proposed deactivation pathways.

	Reaction	rate law	k (M^{-1} s^{-1})	R (M s^{-1})	R/R_t
Termination	$2R^{\bullet} \rightarrow$ R-R	$R_t = k_t[R^{\bullet}]^2$	10^7	2.1×10^{-8}	1
AET,ter	$\mathbf{2}^{\bullet+}$ + $R^{\bullet}$ + Br^- → RBr + **2**	$R_{AET\text{-}ter} = k_{AET\text{-}ter}[\mathbf{2}^{\bullet+}][Br^-][R^{\bullet}]$	3.4×10^{7} [a]	3.9×10^{-6}	1.9×10^{2}
	$\mathbf{2}^{\bullet+}$ + $R^{\bullet}$ + Cl^- → RCl + **2**	$R_{AET\text{-}ter} = k_{AET\text{-}ter}[\mathbf{2}^{\bullet+}][Cl^-][R^{\bullet}]$	7.8×10^{5} [a]	$<9.0\times10^{-8}$	<4.3
ISET	$\mathbf{2}^{\bullet+}Br^-$-C + $R^{\bullet}$ → RBr + **2**	$R_{ISET} = k_{ISET}[\mathbf{2}^{\bullet+}Br^-\text{-}C][R^{\bullet}]$	6.1×10^{3}	5.0×10^{-10}	2.4×10^{-2}
OSET-II	$\mathbf{2}^{\bullet+}$ + $R^{\bullet}$ → R^+ + **2**	$R_{OSET\text{-}II} = k_{OSET\text{-}II}[\mathbf{2}^{\bullet+}][R^{\bullet}]$	3.5×10^{3}	7.7×10^{-8}	3.7
DET	$\mathbf{2}^{\bullet+}Br^-$-C + $R^{\bullet}$ → **2** + Br^- + R^+	$R_{DET} = k_{DET}[\mathbf{2}^{\bullet+}Br^-\text{-}C][R^{\bullet}]$	45	3.7×10^{-12}	1.8×10^{-4}
OSET-I	$\mathbf{2}^{\bullet+}Br^-$-C + $R^{\bullet}$ → **2**-Br^--C + R^+	$R_{OSET\text{-}I} = k_{OSET\text{-}I}[\mathbf{2}^{\bullet+}Br^-\text{-}C][R^{\bullet}]$	32.4	$<2.7\times10^{-12}$	$<1.3\times10^{-4}$

[a] Unit: M^{-2} s^{-1}.[b] Activation of MCiB is much slower than activation of MBiB, $k_{act,MCiB}/k_{act,MBiB} = 2.6\times10^{-3}$. This implies that $[2^{\bullet+}]$ is much smaller with MCiB than with MBiB. For the same reason $[Cl^-] < [Br^-]$. Therefore, $R_{AET\text{-}ter}$ and $R_{AET\text{-}ter}/R_t$ are overestimated.

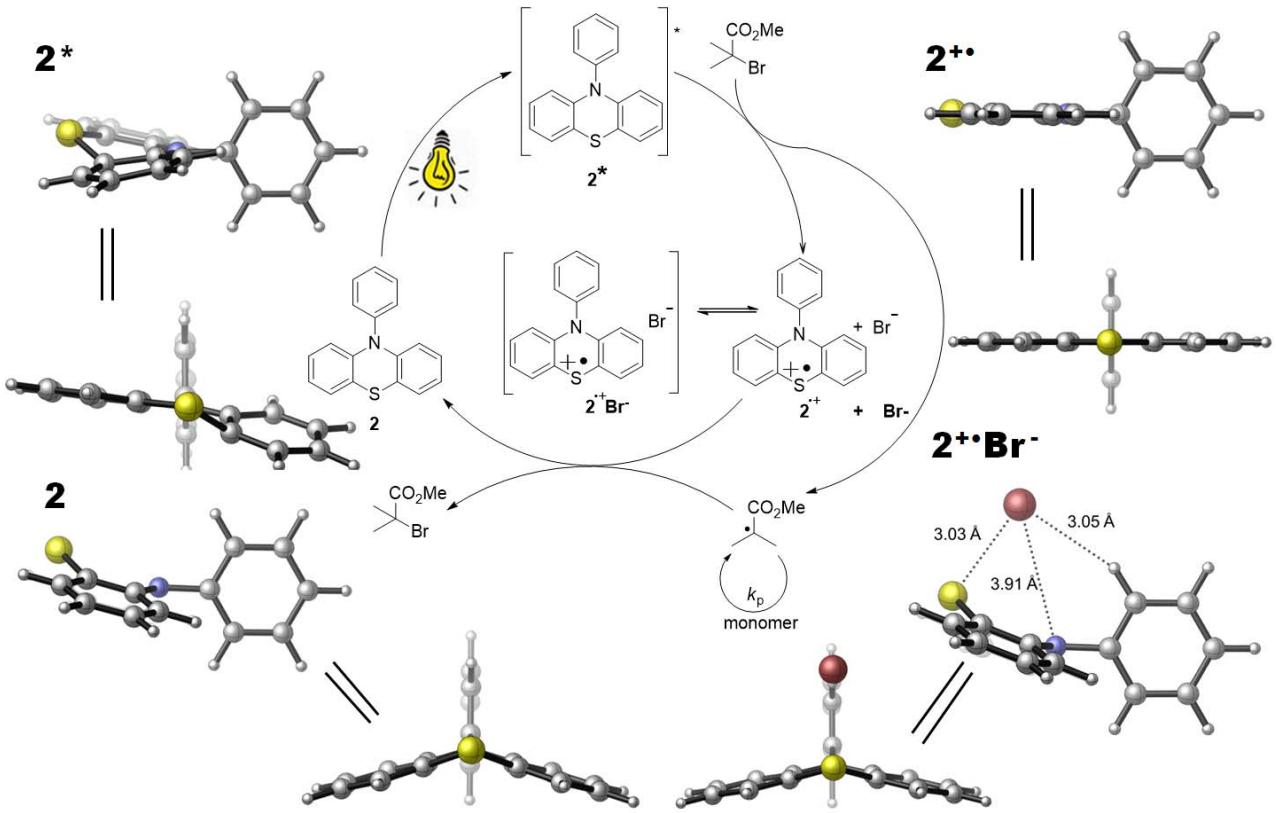

Scheme 5. Proposed overall mechanism for photoinduced metal-free ATRP and optimized geometries of related intermediates, based on DFT calculations.

which is more than 2 orders of magnitude faster than radical-radical termination when RBr is used as initiator or bromide ions are added, as the only possible deactivation pathway.

The same conclusion is reached if $R_{AET\text{-}ter}$ is calculated on the basis of experimental data. In this case, using $\Delta G^{\ddagger} = 29.6$ kcal/mol (Table 4) gives $\Delta G^{\ddagger}_{AET\text{-}ter} = 5.0$ kcal/mol. It follows that $k_{AET\text{-}ter} = 5.8\times10^{6}$ M^{-2} s^{-1}, $R_{AET\text{-}ter} = 6.8\times10^{-7}$ M s^{-1} and $R_{AET\text{-}ter}/R_t = 32$ (see Supporting Information). It is clear that AET-ter is the fastest deactivation pathway and, in particular, at least one order of magnitude faster than all other deactivation reactions. When RCl is used as initiator, AET-ter is only four times faster than termination, which explains why control is lost with a chloride polymerization initiator (EClPA).

Overall Mechanism

A proposed overall mechanism can be constructed by combining all the information from experimental data, LFP measurements, and calculations based on electron transfer (Marcus and further developments) and DFT theories, and is illustrated in Scheme 5. The optimized geometries of related intermediates based on DFT calculations are also shown. After Ph-PTZ **2** is excited to the excited state **2***, a dissociative electron transfer occurs from **2*** to the conventional ATRP initiator (alkyl bromide, MBiB), forming the alkyl radical required to initiate the polymerization. In this process, **2** is oxidized to the radical cation, $\mathbf{2}^{\bullet+}$, which exists in equilibrium with $\mathbf{2}^{\bullet+}\mathbf{Br}^-$. The associative electron transfer (AET-ter) from $\mathbf{2}^{\bullet+}$ to the propagating radical and bromide anion finishes the catalytic cycle to re-

generate ground-state catalyst **2** and polymer chain with bromine as chain-end fidelity.

It is important to note that although the catalytic cycle shown in Scheme 5 is the main pathway for the photoinduced metal-free ATRP process, several background and side reactions also need to be taken into account. Photoinduced homolytic cleavage of the C-Br bond, in the ATRP initiator or polymer chain end, provides alkyl and bromine radicals and both radicals could initiate a polymerization. This background reaction might result in the formation of some dead chains from radical-radical termination. However, this type of termination should be limited. In most cases, the alkyl radicals formed directly from background reaction would abstract the bromine atom either from $\mathbf{2}^{\bullet+}\mathbf{Br}^{-}$ or C-Br in EBPA to regenerate the dormant chain end. Since the excited catalyst **2*** is a strong reductant, it is also plausible that radicals could be reduced to carbanions. However, due to the very low concentration of both radical and catalyst in the excited state, the radical reduction pathway is very slow. Based on the redox property of $\mathbf{2}^{\bullet+}$, it could potentially oxidize Br^- to bromine (Br_2). Upon irradiation Br_2 could generate $Br^{\bullet}$ to initiate the polymerization or Br_2 could add to a double bond to form an active ATRP initiator. In both cases, the formation of Br_2 should not stop the polymerization; however, bromination of the catalyst might turn off its reactivity and **8** might be more easily brominated than **2**.

CONCLUSIONS

The mechanism of photoinduced metal-free ATRP was investigated via a combination of polymerization, kinetics, cyclic voltammetry, laser flash photolysis, dissociative electron transfer, Marcus and DFT calculations. A controlled radical polymerization needs to meet two criteria: fast initiation/activation and efficient deactivation. All selected catalysts are involved in the activation process, and generate alkyl radicals upon irradiation, but not all are efficient deactivators. All phenothiazine derivatives participate in the deactivation process; however, only *N*-aryl phenothiazine derivatives are stable enough to survive until the later stages of the polymerization. Alkyl chlorides could not be successfully used as ATRP initiators and provide an uncontrolled radical polymerization.

Photoinduced metal-free ATRP provides a fascinating avenue to synthesize well-defined polymers in the absence of residual transition metals. For the analyzed phenothiazine-based photocatalysts, activation involves a dissociative electron transfer to RX. Activation rate constants are higher than for classic Cu-based ATRP systems. However, due to a short lifetime of the excited states, activation of RX is quite slow and relatively large amounts of catalyst should be used. Comparison of all reasonable deactivation pathways showed that the most favored reaction route is the termolecular reaction of $\mathbf{2}^{\bullet+}$, $R^{\bullet}$ and Br^-. Similarly to activation reaction, deactivation rate constants are at least as high as that reported for copper complexes, but in this case the rate is severely reduced by the low likelihood of three-center encounters. Therefore, precise control over macromolecular architecture by metal-free ATRP appears to be limited by the establishment of a fairly slow activation/deactivation process.

In order to obtain a well-controlled metal-free ATRP, the catalyst should efficiently absorb photons, and therefore must be excited at the proper wavelength. In addition, photoexcitation should produce a strongly reducing excited state ($E^{e}_{Cat^{\bullet+}/Cat^{*}} \approx$ -2 V vs. SCE), with a sufficiently long lifetime ($\tau_0 \geq 5$ ns) and high quantum efficiency ($\Phi_F \geq 0.01$) to ensure efficient activation of the R-X bond. The generated radical cation should also be stable (lifetime >> 10 s) and have a high reduction potential ($E^{e}_{Cat^{\bullet+}/Cat^{*}} \approx 0.8$ V vs. SCE) to ensure the quick oxidative trapping of $R^{\bullet}$ and Br^-.

ASSOCIATED CONTENT

Supporting Information. Experimental procedures for preparation, characterization of all compounds, additional experimental data, supplementary figures, detailed kinetics and DFT calculations. This material is available free of charge via the Internet at http://pubs.acs.org.

AUTHOR INFORMATION

Corresponding Author

A.G.: armando.gennaro@unipd.it
P.L.: pengliu@pitt.edu
K.M.: km3b@andrew.cmu.edu

Notes

The authors declare no competing financial interests.

ACKNOWLEDGMENT

We thank the NSF (CHE-1400052) and members of the CRP Consortium (K.M., X.P., N.M.), University of Padova (A.G., A.A.I., M.F.), Fondazione Ing. Aldo Gini (M.F.). DFT Calculations were performed at the Center for Simulation and Modeling at the University of Pittsburgh and the Extreme Science and Engineering Discovery Environment (XSEDE) supported by NSF (P.L., C.F.). We also acknowledge Dr. Michelle Coote for helpful discussion.

REFERENCES

1. a) Goto, A.; Fukuda, T. *Prog. Polym. Sci.* **2004**, *29*, 329-385; b) Braunecker, W. A.; Matyjaszewski, K. *Prog. Polym. Sci.* **2007**, *32*, 93-146; c) Matyjaszewski, K.; Davis, T. P. *Handbook of radical polymerization*; Wiley Online Library, 2002.

2. a) Nicolas, J.; Guillaneuf, Y.; Lefay, C.; Bertin, D.; Gigmes, D.; Charleux, B. *Prog. Polym. Sci.* **2013**, *38*, 63-235; b) Hawker, C. J.; Bosman, A. W.; Harth, E. *Chem. Rev.* **2001**, *101*, 3661-3688.

3. a) Wang, J.-S.; Matyjaszewski, K. *J. Am. Chem. Soc.* **1995**, *117*, 5614-5615; b) Kato, M.; Kamigaito, M.; Sawamoto, M.; Higashimura, T. *Macromolecules* **1995**, *28*, 1721-1723; c) Patten, T. E.; Xia, J.; Abernathy, T.; Matyjaszewski, K. *Science* **1996**, *272*, 866-868; d) Matyjaszewski, K.; Xia, J. *Chem. Rev.* **2001**, *101*, 2921-2990; e) Matyjaszewski, K.; Tsarevsky, N. V. *J. Am. Chem. Soc.* **2014**, *136*, 6513-6533; f) Matyjaszewski, K. *Macromolecules* **2012**, *45*, 4015-4039.

4. a) Chiefari, J.; Chong, Y. K.; Ercole, F.; Krstina, J.; Jeffery, J.; Le, T. P. T.; Mayadunne, R. T. A.; Meijs, G. F.; Moad, C. L.; Moad, G.; Rizzardo, E.; Thang, S. H. *Macromolecules* **1998**, *31*, 5559-5562; b) Hill, M. R.; Carmean, R. N.; Sumerlin, B. S. *Macromolecules* **2015**, *48*, 5459-5469.

5. a) De Paoli, P.; Isse, A. A.; Bortolamei, N.; Gennaro, A. *Chem. Commun.* **2011**, *47*, 3580-3582; b) Matyjaszewski, K.; Patten, T. E.; Xia, J. *J. Am. Chem. Soc.* **1997**, *119*, 674-680.

6. Pintauer, T.; Matyjaszewski, K. *Chem. Soc. Rev.* **2008**, *37*, 1087-1097.

7. Jakubowski, W.; Matyjaszewski, K. *Angew. Chem. Int. Ed.* **2006**, *45*, 4482-4486.

8. Matyjaszewski, K.; Jakubowski, W.; Min, K.; Tang, W.; Huang, J.; Braunecker, W. A.; Tsarevsky, N. V. *Proc. Natl. Acad. Sci. U.S.A.* **2006**, *103*, 15309-15314.

9. a) Konkolewicz, D.; Wang, Y.; Krys, P.; Zhong, M.; Isse, A. A.; Gennaro, A.; Matyjaszewski, K. *Polym. Chem.* **2014**, *5*, 4396-4417;

b) Konkolewicz, D.; Wang, Y.; Zhong, M.; Krys, P.; Isse, A. A.; Gennaro, A.; Matyjaszewski, K. *Macromolecules* **2013**, *46*, 8749-8772.

10. Rosen, B. M.; Percec, V. *Chem. Rev.* **2009**, *109*, 5069-5119.

11. a) Magenau, A. J. D.; Strandwitz, N. C.; Gennaro, A.; Matyjaszewski, K. *Science* **2011**, *332*, 81-84; b) Park, S.; Chmielarz, P.; Gennaro, A.; Matyjaszewski, K. *Angew. Chem. Int. Ed.* **2015**, *54*, 2388-2392; c) Bortolamei, N.; Isse, A. A.; Magenau, A. J. D.; Gennaro, A.; Matyjaszewski, K. *Angew. Chem. Int. Ed.* **2011**, *50*, 11391-11394.

12. a) Konkolewicz, D.; Schroder, K.; Buback, J.; Bernhard, S.; Matyjaszewski, K. *ACS Macro Lett.* **2012**, *1*, 1219-1223; b) Ribelli, T. G.; Konkolewicz, D.; Pan, X.; Matyjaszewski, K. *Macromolecules* **2014**, *47*, 6316-6321; c) Mosnáček, J.; Ilčíková, M. *Macromolecules* **2012**, *45*, 5859 − 5865; d) Anastasaki, A.; Nikolaou, V.; Zhang, Q.; Burns, J.; Samanta, S. R.; Waldron, C.; Haddleton, A. J.; McHale, R.; Fox, D.; Percec, V.; Wilson, P.; Haddleton, D. M. *J. Am. Chem. Soc.* **2014**, *136*, 1141-1149; e) Pan, X.; Malhotra, N.; Simakova, A.; Wang, Z.; Konkolewicz, D.; Matyjaszewski, K. *J. Am. Chem. Soc.* **2015,** *137*, 15430 - 15433; f) Dadashi-Silab, S.; Atilla Tasdelen, M.; Yagci, Y. *J. Polym. Sci. A Polym. Chem.* **2014**, *52*, 2878-2888; g) Ciftci, M.; Tasdelen, M. A.; Li, W.; Matyjaszewski, K.; Yagci, Y. *Macromolecules* **2013**, *46*, 9537-9543; h) Tasdelen, M. A.; Ciftci, M.; Yagci, Y. *Macromol. Chem. Phys.* **2012**, *213*, 1391-1396; i) Tasdelen, M. A.; Uygun, M.; Yagci, Y. *Macromol. Rapid Commun.* **2011**, *32*, 58-62; j) Tasdelen, M. A.; Uygun, M.; Yagci, Y. *Macromol. Chem. Phys.* **2010**, *211*, 2271-2275; k) Kwak, Y.; Matyjaszewski, K. *Macromolecules* **2010**, *43*, 5180-5183.

13. a) Pan, X.; Malhotra, N.; Zhang, J.; Matyjaszewski, K. *Macromolecules* **2015**, *48*, 6948-6954; b) Yang, Q.; Dumur, F.; Morlet-Savary, F.; Poly, J.; Lalevée, J. *Macromolecules* **2015**, *48*, 1972-1980.

14. Fors, B. P.; Hawker, C. J. *Angew. Chem. Int. Ed.* **2012**, *51*, 8850 − 8853.

15. a) Meyer, T. J. *Accounts of Chemical Research* **1989**, *22*, 163-170; b) Lalrempuia, R.; McDaniel, N. D.; Müller-Bunz, H.; Bernhard, S.; Albrecht, M. *Angew. Chem. Int. Ed.* **2010**, *49*, 9765-9768; c) DiSalle, B. F.; Bernhard, S. *J. Am. Chem. Soc.* **2011**, *133*, 11819-11821.

16. Kalyanasundaram, K. *Coord. Chem. Rev.* **1982**, *46*, 159-244.

17. Howerton, B. S.; Heidary, D. K.; Glazer, E. C. *J. Am. Chem. Soc.* **2012**, *134*, 8324-8327.

18. a) Kärkäs, M. D.; Matsuura, B. S.; Stephenson, C. R. J. *Science* **2015**, *349*, 1285-1286; b) Le, C. C.; MacMillan, D. W. C. *J. Am. Chem. Soc.* **2015**, *137*, 11938-11941; c) Nawrat, C. C.; Jamison, C. R.; Slutskyy, Y.; MacMillan, D. W. C.; Overman, L. E. *J. Am. Chem. Soc.* **2015**, *137*, 11270-11273; d) Jin, J.; MacMillan, D. W. C. *Nature* **2015**, *525*, 87-90; e) Terrett, J. A.; Cuthbertson, J. D.; Shurtleff, V. W.; MacMillan, D. W. C. *Nature* **2015**, *524*, 330-334; f) Prier, C. K.; Rankic, D. A.; MacMillan, D. W. C. *Chem. Rev.* **2013**, *113*, 5322-5363; g) Romero, N. A.; Margrey, K. A.; Tay, N. E.; Nicewicz, D. A. *Science* **2015**, *349*, 1326-1330; h) Griffin, J. D.; Zeller, M. A.; Nicewicz, D. A. *J. Am. Chem. Soc.* **2015**, *137*, 11340-11348.

19. a) Lalevée, J.; Peter, M.; Dumur, F.; Gigmes, D.; Blanchard, N.; Tehfe, M.-A.; Morlet-Savary, F.; Fouassier, J. P. *Chem. Eur. J.* **2011**, *17*, 15027-15031; b) Lalevée, J.; Blanchard, N.; Tehfe, M.-A.; Morlet-Savary, F.; Fouassier, J. P. *Macromolecules* **2010**, *43*, 10191-10195; c) Ogawa, K. A.; Goetz, A. E.; Boydston, A. J. *J. Am. Chem. Soc.* **2015**, *137*, 1400-1403; d) Xiao, P.; Zhang, J.; Dumur, F.; Tehfe, M. A.; Morlet-Savary, F.; Graff, B.; Gigmes, D.; Fouassier, J. P.; Lalevée, J. *Prog. Polym. Sci.* **2015**, *41*, 32-66; e) Perkowski, A. J.; You, W.; Nicewicz, D. A. *J. Am. Chem. Soc.* **2015**, *137*, 7580-7583.

20. a) Xu, J.; Jung, K.; Atme, A.; Shanmugam, S.; Boyer, C. *J. Am. Chem. Soc.* **2014**, *136*, 5508-5519; b) Shanmugam, S.; Xu, J.; Boyer, C. *J. Am. Chem. Soc.* **2015**, *137*, 9174-9185; c) Shanmugam, S.; Xu, J.; Boyer, C. *Chem. Sci.* **2015**, *6*, 1341-1349; d) Xu, J.; Shanmugam, S.; Duong, H. T.; Boyer, C. *Polym. Chem.* **2015**, *6*, 5615-5624; e) Shanmugam, S.; Boyer, C. *J. Am. Chem. Soc.* **2015**, *137*, 9988-9999; f) Yeow, J.; Xu, J.; Boyer, C. *ACS Macro Lett.* **2015**, *4*, 984-990; g) Chen, M.; MacLeod, M. J.; Johnson, J. A. *ACS Macro Lett.* **2015**, *4*, 566-569.

21. Treat, N. J.; Fors, B. P.; Kramer, J. W.; Christianson, M.; Chiu, C.-Y.; Alaniz, J. R. d.; Hawker, C. J. *ACS Macro Lett.* **2014**, *3*, 580-584.

22. Poelma, J. E.; Fors, B. P.; Meyers, G. F.; Kramer, J. W.; Hawker, C. J. *Angew. Chem. Int. Ed.* **2013**, *52*, 6844-6848.

23. Treat, N. J.; Sprafke, H.; Kramer, J. W.; Clark, P. G.; Barton, B. E.; Read de Alaniz, J.; Fors, B. P.; Hawker, C. J. *J. Am. Chem. Soc.* **2014**, *136*, 16096-16101.

24. Pan, X.; Lamson, M.; Yan, J.; Matyjaszewski, K. *ACS Macro Lett.* **2015**, *4*, 192-196.

25. Kaur, A.; Ribelli, T. G.; Schröder, K.; Matyjaszewski, K.; Pintauer, T. *Inorg. Chem.* **2015**, *54*, 1474-1486.

26. a) Lin, C. Y.; Coote, M. L.; Gennaro, A.; Matyjaszewski, K. *J. Am. Chem. Soc.* **2008**, *130*, 12762-12774; b) Isse, A. A.; Bortolamei, N.; De Paoli, P.; Gennaro, A. *Electrochim. Acta* **2013**, *110*, 655-662.

27. a) Marcus, R. A. *J. Chem. Phys* **1956**, *24*, 966-978; b) Pause, L.; Robert, M.; Savéant, J.-M. *J. Am. Chem. Soc.* **2000**, *122*, 9829-9835; c) Saveant, J. M. *J. Am. Chem. Soc.* **1987**, *109*, 6788-6795; d) Saveant, J. M. *J. Am. Chem. Soc.* **1992**, *114*, 10595-10602.

28. Isse, A. A.; Gennaro, A.; Lin, C. Y.; Hodgson, J. L.; Coote, M. L.; Guliashvili, T. *J. Am. Chem. Soc.* **2011**, *133*, 6254-6264.

29. Flamigni, L.; Barbieri, A.; Sabatini, C.; Ventura, B.; Barigelletti, F. In *Photochemistry and Photophysics of Coordination Compounds II*; Balzani, V., Campagna, S., Eds.; Springer Berlin Heidelberg, 2007; Topics in Current Chemistry, Vol. 281.

30. a) Wallentin, C.-J.; Nguyen, J. D.; Finkbeiner, P.; Stephenson, C. R. J. *J. Am. Chem. Soc.* **2012**, *134*, 8875-8884; b) Nguyen, J. D.; Tucker, J. W.; Konieczynska, M. D.; Stephenson, C. R. J. *J. Am. Chem. Soc.* **2011**, *133*, 4160-4163.

31. a) Lin, C. Y.; Coote, M. L.; Petit, A.; Richard, P.; Poli, R.; Matyjaszewski, K. *Macromolecules* **2007**, *40*, 5985-5994; b) Nanda, A. K.; Matyjaszewski, K. *Macromolecules* **2003**, *36*, 8222-8224.

32. Pérez-Prieto, J.; Miranda, M. A. In *Encyclopedia of Radicals in Chemistry, Biology and Materials*; John Wiley & Sons, Ltd, 2012.

33. Surry, D. S.; Buchwald, S. L. *Chem. Sci.* **2011**, *2*, 27-50.

34. Crivello, J. V. *J. Polym. Sci. A Polym. Chem.* **2008**, *46*, 3820-3829.

35. a) Tehfe, M.-A.; Lalevée, J.; Morlet-Savary, F.; Graff, B.; Blanchard, N.; Fouassier, J.-P. *ACS Macro Lett.* **2012**, *1*, 198-203; b) Kolosov, D.; Adamovich, V.; Djurovich, P.; Thompson, M. E.; Adachi, C. *J. Am. Chem. Soc.* **2002**, *124*, 9945-9954.

36. Lifetime of Ph-PTZ* is 2.3 ns, measued in MeCN, see: Discekici, E. H.; Treat, N. J.; Poelma, S. O.; Mattson, K. M.; Hudson, Z. M.; Luo, Y.; Hawker, C. J.; de Alaniz, J. R. *Chem. Commun.* **2015**, 51, 11705.

37. a) Isse, A. A.; Sandonà, G.; Durante, C.; Gennaro, A. *Electrochim. Acta* **2009**, *54*, 3235-3243; b) Costentin, C.; Robert, M.; Savéant, J.-M. *J. Am. Chem. Soc.* **2003**, *125*, 10729-10739; c) Isse, A. A.; Gennaro, A. *J. Phys. Chem. A* **2004**, *108*, 4180-4186; d) Cardinale, A.; Isse, A. A.; Gennaro, A.; Robert, M.; Savéant, J.-M. *J. Am. Chem. Soc.* **2002**, *124*, 13533-13539; e) Andrieux, C. P.; Le Gorande, A.; Saveant, J. M. *J. Am. Chem. Soc.* **1992**, *114*, 6892-6904; f) Andrieux, C. P.; Gallardo, I.; Savaent, J. M.; Su, K. B. *J. Am. Chem. Soc.* **1986**, *108*, 638-647.

38. Pause, L.; Robert, M.; Savéant, J.-M. *J. Am. Chem. Soc.* **2001**, *123*, 4886-4895.

39. Isse, A. A.; Lin, C. Y.; Coote, M. L.; Gennaro, A. *J. Phys. Chem. B* **2011**, *115*, 678-684.

40. Saucin, M.; Van de Vorst, A. *Radiat. Environ. Biophys.* **1980**, *17*, 159-168.

41. Jung, S. O.; Kim, Y.-H.; Kim, H.-S.; Kwon, S.-K.; Oh, H.-Y. *Mol. Cryst. Liq. Cryst.* **2006**, *444*, 95-101.

42. Rehm, D.; Weller, A. *Isr. J. Chem.* **1970**, *8*, 259-271.

43. Konkolewicz, D.; Krys, P.; Góis, J. R.; Mendonça, P. V.; Zhong, M.; Wang, Y.; Gennaro, A.; Isse, A. A.; Fantin, M.; Matyjaszewski, K. *Macromolecules* **2014**, *47*, 560-570.

44. Lorandi, F.; Fantin, M.; Isse, A. A.; Gennaro, A. *Polymer* **2015**, *72*, 238-245.

45. Fantin, M.; Isse, A. A.; Gennaro, A.; Matyjaszewski, K. *Macromolecules* **2015**, *48*, 6862-6875.

46. Turro, N. J., Modern Molecular Photochemistry 1978, University Science Books, Herndon, VA, USA.

47. Bortolamei, N.; Isse, A. A.; Gennaro, A. *Electrochim. Acta* **2010**, *55*, 8312-8318.

48. For computational studies on Cu-catalyzed ATRP reactions, see refs 26a and 28.

49. For computational studies of photoredox reactions with transition metal-based catalysts: (a) Gutierrez, O.; Tellis, J. C.; Primer, D. N.; Molander, G. A.; Kozlowski, M. C. *J. Am. Chem. Soc.* **2015**, 137, 4896 − 4899. (b) Demissie, T. B.; Ruud, K.; Hansen, J. H. *Organometallics*, **2015**, 34, 4218 − 4228.

50. a) Pan, D.; Phillips, D. L. *J. Phys. Chem. A* **1999**, *103*, 4737-4743; b) Okamoto, T.; Kuratsu, M.; Kozaki, M.; Hirotsu, K.; Ichimura, A.; Matsushita, T.; Okada, K. *Org. Lett.* **2004**, *6*, 3493-3496.

51. The relative stabilities of **2**$^{\bullet+}$, **2**$^{\bullet+}$**Br**$^{-}$**-C**, and **2**$^{\bullet+}$**Br**$^{-}$**-I** are computed at different level of theories to benchmark the accuracy of the computational methods. The method used in this study gives good agreement with the high-level DF-LUCCSD(T)/cc-pVTZ calculations. The computed stability of the ion pair complexes is also affected by the implicit solvation model. Calculations using the CPCM solvation model in place of SMD predicted a more favorable dissociation of the **2**$^{\bullet+}$**Br**$^{-}$ ion pair due to greater stability of the bromide anion in solution. See the Supporting Information for details.

52. Among the two low energy isomers of ion pair **2**$^{\bullet+}$**Br**$^{-}$, only the covalent isomer **2**$^{\bullet+}$**Br**$^{-}$**-C** is considered in the calculations of the deactivation mechanisms. Due to the weak interactions between **2**$^{\bullet+}$ and Br− in the ionic isomer of the ion pair, the reactivity of **2**$^{\bullet+}$**Br**$^{-}$**-I** is expected to be similar to the separated catalyst radical cation and halide anion.

53. Savéant, J.-M. *J. Electroanal. Chem.* **2000**, *485*, 86-88.

54. Shine, H. J.; Silber, J. J.; Bussey, R. J.; Okuyama, T. *J. Org. Chem.* **1972**, *37*, 2691-2697.

55. (a) R.C. Tolman, Statistical Mechanics, Chemical Catalog Co, New York, 1927, p. 247. (b) J.R. Partington, An Advanced Treatise on Physical Chemistry, vol. 1, Longmans, London, 1967, p. 292. (c) J.W. Moore, R.N. Pearson, Kinetics and Mechanism, vol. 131, Wiley, New York, 1981, p. 130.

56. a) Matyjaszewski, K.; Paik, H.-j.; Zhou, P.; Diamanti, S. J. *Macromolecules* **2001**, *34*, 5125-5131; b) Tang, W.; Kwak, Y.; Braunecker, W.; Tsarevsky, N. V.; Coote, M. L.; Matyjaszewski, K. *J. Am. Chem. Soc.***2008**, *130*, 10702-10713; c) Zerk, T. J.; Bernhardt, P. V. *Inorg. Chem.* **2014**, *53*, 11351-11353.

Insert Table of Contents artwork here